Chapter 4

Cinchona Alkaloid Derivatives modified Fe_3O_4 Nanoparticles for Enantioselective Ring Opening of *meso*- Cyclic Anhydrides

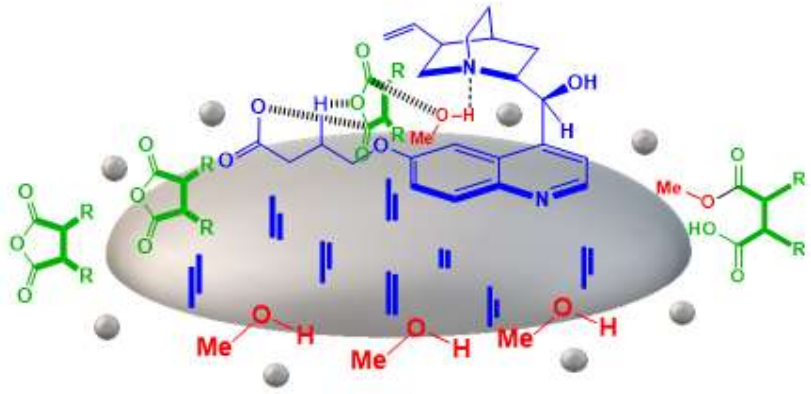

Published in: ***New Journal of Chemistry*****, 2022,**46**, 2495-2507**

4.1. Introduction

Enantioselective meso-cyclic anhydride ring opening or desymmetrization of cyclic anhydride is one of the most important protocols in the field of asymmetric synthesis. [1-5] It allows the direct accesses of product with multiple stereocentres in a single step with high stereoselectivity (almost 99% ee) and yield.[6] Due to this protocol, many steps (eg. protection-deprotection of essential functional groups) and precious chiral auxiliaries involved in a total synthesis can be saved. Total synthesis of (+)-biotin (a member of series of water-soluble vitamin B, widely distributed in microorganisms, animals, and plants and necessary for the metabolism of fatty acids, α-amino acids, and sugars) through the Goldenberg-Strenbatch approach is a well-known example (Scheme 1).[7, 8]

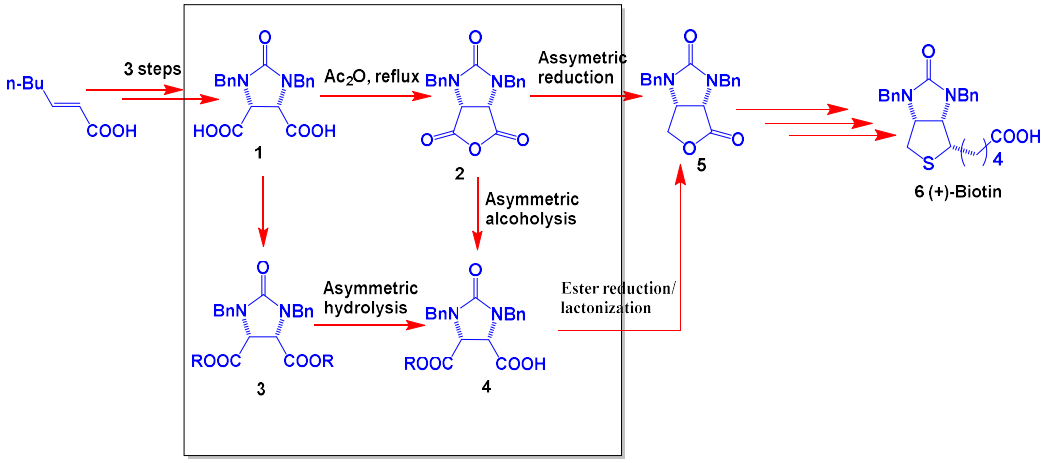

Scheme 1 Total synthesis of (+)-biotin by Goldenberg-Strenbatch approach. [7,8]

As can be seen from Scheme 1 the monoesterification of diacid **1** to **4** is very difficult and the available methods are inefficient to achieve complete conversion and selectivity. For example, (i) mineral acid-catalyzed esterification in which diacid treated with a stoichiometric amount of alcohol lack the selectivity of the desired monoester and yield a mixture of monoester, diester, and unreacted alcohol [9, 10] (ii) the reactivity of the two carboxylic groups can be differentiated by adsorbing the diacid on the suitable support (like alumina or silica). By chemisorption of one of the two carboxylate ions on the surface (either monodentate or bidentate) of support make the other group away which can be esterified easily using the esterification toolkit.[11] However, monocarboxylate desorption from the surface is time-consuming, and different dicarboxylic acids may have different affinities for the support

depending on the hydrocarbon chain length. Hence, substrate-wise special methods must be developed for this purpose. Unanimity to have a single protocol lacks (iii) enzyme-mediated methods are designed for these kinds of protocols. [12, 13] But they have their drawbacks regarding stability and storage of costly available enzymes with their recovery. Another method to synthesize monoester is to convert diacid completely into diester with excess alcohol under normal esterification conditions. Then the resulting diester **3** is asymmetrically hydrolyzed with lipase type enzymes into chiral hemiester **4**. However, this approach is not feasible and riddled with extra steps and total synthesis cost.

One of the most innovative ideas towards the synthesis of hemiester is to start with *meso*-cyclic anhydride **2** instead of diester **3**. ERO of such meso-cyclic anhydride **2** would result in chiral hemiester **4** in a single step. [14] The chiral hemiester can easily be converted into lactone **5** having desired configuration by stereoselective reduction of either ester or carboxylic group using a suitable reducing agent (like Noyori's BINAL-H) and cyclization.[15] Many approaches have been developed for the ERO of anhydride to date. However, they have met with limited success in terms of % yield, selectivity, and applicability to all types of anhydrides. For example, Seebach developed chiral Ti-TADDOLate systems (**7**), [16,17] Shibasaki developed Ni_2-Schiff base catalyst **(8),** [18] and Kunieda developed Li complexes of chiral N-sulphonyl amino alcohols (**9**). [19,20] However, they are all costly, their high mol % required, and not equally effective for the ring-opening of all kinds of anhydrides (like mono-, bi- and tricyclic anhydrides).

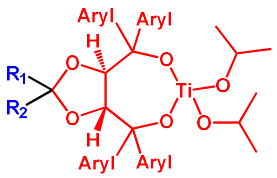

R_1=R_2= Methyl, Aryl=Phenyl
R_1=Phenyl, R_2=H, Aryl=Phenyl
R_1=R_2= Methyl, Aryl=α-$C_{10}H_7$
R_1=R_2= Methyl, Aryl=β-$C_{10}H_7$
R_1=R_2=Aryl=Phenyl

7

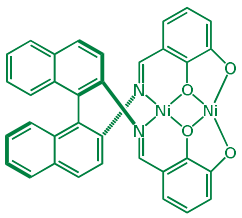

(R)-Ni2-(Schiff base)

8

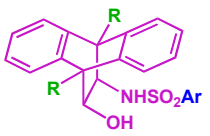

R=Me, H
Ar= Ph,

9

Naturally occurring cinchona alkaloids and their derivatives are widely studied for this purpose. [21-23] Due to the legacy of having a wide array of functionalities and unique molecular framework, these compounds are considered as small molecular chiral catalyst having

"privileged structures" by Jacobson.[24] Cinchona alkaloids have a common unique molecular structure like the aromatic quinoline ring system is connected with aliphatic bicyclic quinuclidine moiety through –CH(OH)- linkage which bestows the whole structure flexible and adopts various conformations due to rotation around this bond. The spatial arrangement of hydroxyl group and hydrogen at C9 and C8 respectively, resulting in multiple diastereomers and quasi-enatiomers. [25, 26] In 1985, Oda et al., for the first time, reported ERO of prochiral 2,4-dimethyl glutaric anhydride **(10)** using cinchona alkaloids.[27] They carried out alcoholysis of **10** in the presence of 10 mol% of quinidine using 4.0 equiv. of MeOH (*w.r.t* **10**) in toluene as a solvent at RT. They achieved 67% ee of hemiester **11** at the end of 4 days. Aitken et al. carried out the alcoholysis of anhydride **12** in the presence of catalytic amount (0.1 to 0.5 equiv. w.r.t anhydride) of quinidine by using 3.0 equiv. of MeOH in toluene at RT. They achieved 44 -67% ee of hemiester on increasing the amount of catalyst.[28] The major lacuna of these protocols is that they are selective for a combination of catalysts and substrates. Oda's protocol is highly efficient for the alcoholysis of glutaric anhydrides with enantioselectivity of about 70%. However, it is less efficient for succinic anhydrides. While Aitken's protocol is efficient for tricyclic succinic anhydrides and achieves a maximum of 67% ee. [29] In 1999, Bolm et al. improved this protocol and carried the reaction at -55 ^{o}C in the presence of a stoichiometric amount of quinidine in toluene as a solvent. They achieved a high % yield and selectivity (above 90% ee) within 60 h. Interestingly, quinine and quinidine catalyzed reactions yield opposite enantiomers.[30, 31] This protocol is easy and highly effective for most of the anhydrides; however, it is less selective for **13** and not effective for sterically hindered succinic anhydrides **14, 15** and **16**.

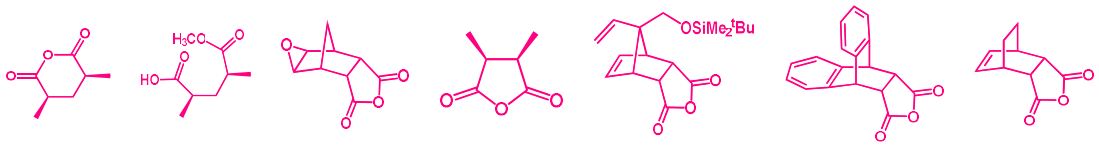

10 **11** **12** **13** **14** **15** **16**

From this discussion, it can be concluded that the present ERO protocols have the following lacunae (i) they are carried out at very low temperatures ranging from -40 to -55 ^{o}C (ii) toxic solvents like CCl_4 and toluene or their 1:1 mixture is generally used as a solvent. If the reaction

is carried out in excess alcohol like polar solvents (which may be one of the reactants also), the selectivity of the end product has to be compromised (iii) if the chiral mediators like enzymic or non-enzymic compounds are used then they are very costly, and their recovery becomes an issue, (iv) if the reaction is carried out in the presence of naturally occurring cinchona alkaloids and their derivatives, universal applicability of the protocol to all the anhydride substrates with equally high selectivity becomes an issue. The parameters like spatial arrangement of functional groups, the amount of catalyst involved in the reaction, solvent polarity, the molecular framework of the substrate anhydrides, recovery and recycling of the catalyst, reaction temperature, etc. must be regulated to achieve high selectivity.

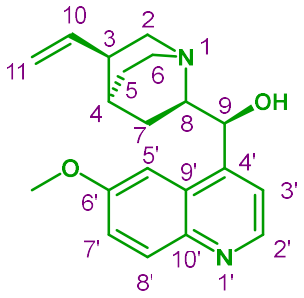

Fig. 1. Molecular frame-work of quinidine.

This work aims to create a chiral surface by chemisorbing the asymmetric molecules from the cinchona alkaloid class. It would be interesting to study the fate of ERO by alcoholysis to form chiral hemiester when carried out over such chiral surfaces. Fe_3O_4 NPs are the most suitable materials for surface modification and the ease of chiral catalyst recovery and recycling. Literature survey shows that most of the ERO by alcoholysis is carried out in the presence of quinidine, a member of the cinchona alkaloid class, as a catalyst. From the structural point of view, it is meaningful to exploit $–OCH_3$ group attached at C6' of quinoline ring of quinidine to make the molecule suitable for surface adsorption and take advantage of the whole cinchona molecular framework for chiral induction (Fig. 1) But the main hindrance is the short chain-length of the $–OCH_3$ group, which makes it unsuitable for surface interactions. Instead, the carboxylic acid group is the most suitable to interact with the surface Fe^{2+}/Fe^{3+} ions either in monodentate or bidentate modes. Considering these aspects, the $-OCH_3$ group at C6' is replaced by $–O(CH_2)_3COOH$ group to induce flexibility at the end (Scheme 2). The final

modified quinidine derivative **19** (mQD) acts as a capping agent during the synthesis of Fe_3O_4 NPs.

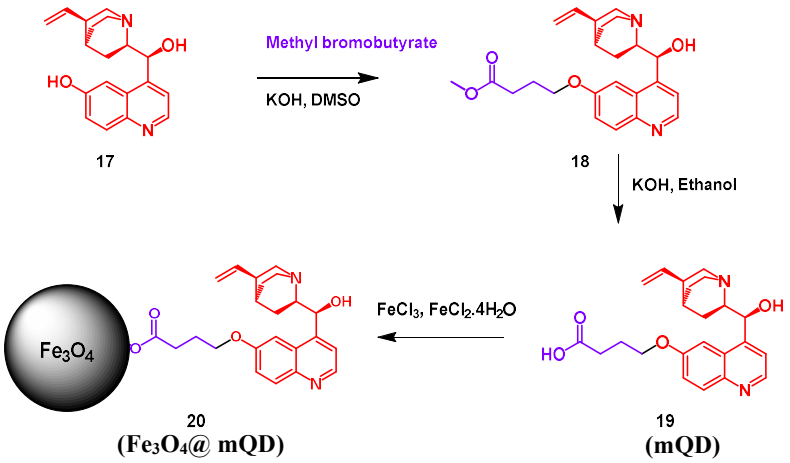

Scheme 2. Preparation of modified quinidine supported on Fe_3O_4 magnetic nanoparticles (Fe_3O_4 @mQD NPs).

The developed catalytic system has an added advantage of heterogeneous catalysis and easy recovery at the end of the reaction through magnetic separation (Scheme 2). We have selected mainly succinic anhydrides having a different steric and molecular framework for which the above discussed well-established protocols have some limitations. We have demonstrated that the developed chiral mediator is effective for the ERO of succinic anhydrides and substituted chiral glutaric anhydrides. We optimized the reaction parameters like solvents, temperature, catalyst loading, and reaction time for ERO. We found that the maximum yield of chiral hemiester (more than 90%) and % ee (up to 98%) resulted when the reaction was carried out at -45 ^oC with 10 mol equiv. of MeOH in diethyl ether as a solvent in the presence of a catalytic amount of Fe_3O_4@mQD NPs. Various analytical techniques are employed to explore the probable mechanism for the high enantioselectivity on chemisorption of mQD. Also, we have demonstrated the pilot-scale production of selected chiral hemiester, and the flow-sheet diagram for the same is presented.

4.2. Results and discussion

The synthesized Fe_3O_4@mQD NPs were characterized by powder XRD to check the material's phase purity, particle size, and crystallinity. The X-ray diffraction peaks at 2θ values of 31.5, 36.2, 43.7, 53.4, 57.5 and 63.0^o correspond to the (220), (311), (400), (422), (511) and (440) planes, respectively (JCPDS no. 82-1533), confirming the magnetite phase of Fe_3O_4 NPs with

inverted spinel structure (Fig. 2a). The particle size was calculated by the Debye-Scherrer formula ($L=0.9\lambda/\beta\cos\theta$) [32] and the FWHM (Full Width at Half Maximum) value of the major peak for (311) planes is in the range of 22.73 nm. XRD pattern remains unaltered on surface adsorption of mQD. The nitrogen adsorption-desorption isotherms for the synthesized Fe_3O_4@mQD NPs, their calculated BET surface area, and pore volume are presented in Fig. 2b and Table 1. It can be observed from Fig. 2(b) that the isotherms of Fe_3O_4@mQD NPs are almost similar to that of type IV (BDDT classification) with the H4 type of hysteresis loop in which the two branches are nearly horizontal and parallel over a wide range of relative pressures (P/Po). In this case, the quantity of gas adsorbed increases with an increase in P/Po. The type H4 loop is often associated with narrow slit-like pores. [33,34] The adsorption average pore width (4 V $Å^{-1}$ by BET) values indicate a mesoporous material. The BET surface area and pore size studies reveal that the material is suitable for catalytic activities.

Table 1. BET surface characterization of as-synthesized Fe_3O_4@mQD NPs.

	Parameters	**Results**
1	BET surface area	57.55m^2/g
2	Adsorption average pore diameter (4V/A)	115.28Å
3	Adsorption average pore width (4V/Aby BET)	129.45Å
4	Volume in pores	0.0015cm^3/g
5	Total volume in pores	0.16 cm^3/g

The structure and morphology of the sample were observed directly by Field-Effect Scanning Electron Microscopy (FESEM) and Transmission Electron Microscopy (TEM) (Fig. 2c-f). It can be observed from Fig. 2 that Fe_3O_4@mQD NPs manifest spherical morphology in a size range of 2 -10 nm. The highly crystalline nature of the material is confirmed from the Selected Area Electron Diffraction (SAED) pattern. The lattice fringes of the exposed planes (400) are spaced between 0.20 nm distances.

FTIR spectroscopy is one of the best tools to study ligand molecules' interactions with the host surface. [35-37] Figure 2g shows the FTIR spectra of mQD and Fe_3O_4@mQD. The vibrations at 1590 and 1430 cm^{-1} correspond to ν_{as} and ν_s carboxylate stretching in free mQD. On coordination with surface Fe^{2+}/Fe^{3+} ions, the ν_{as} increases to 1620 cm^{-1} while that of ν_s

decreases to 1407 cm^{-1}. On comparing Δ ($\nu_{as(COO^-)}$ - $\nu_{s(COO^-)}$) with Δ' ($\nu'_{as(COO^-)}$ - $\nu'_{s(COO^-)}$), Δ < Δ' was established (where Δ indicates the difference in the absorption bands for pristine Fe_3O_4 NPs while Δ' indicates the same for Fe_3O_4@mQD) suggesting monodentate coordination of carboxylate ions of mQD with the surface Fe^{2+}/Fe^{3+} ions under the conditions of chemical synthesis (Scheme 2).

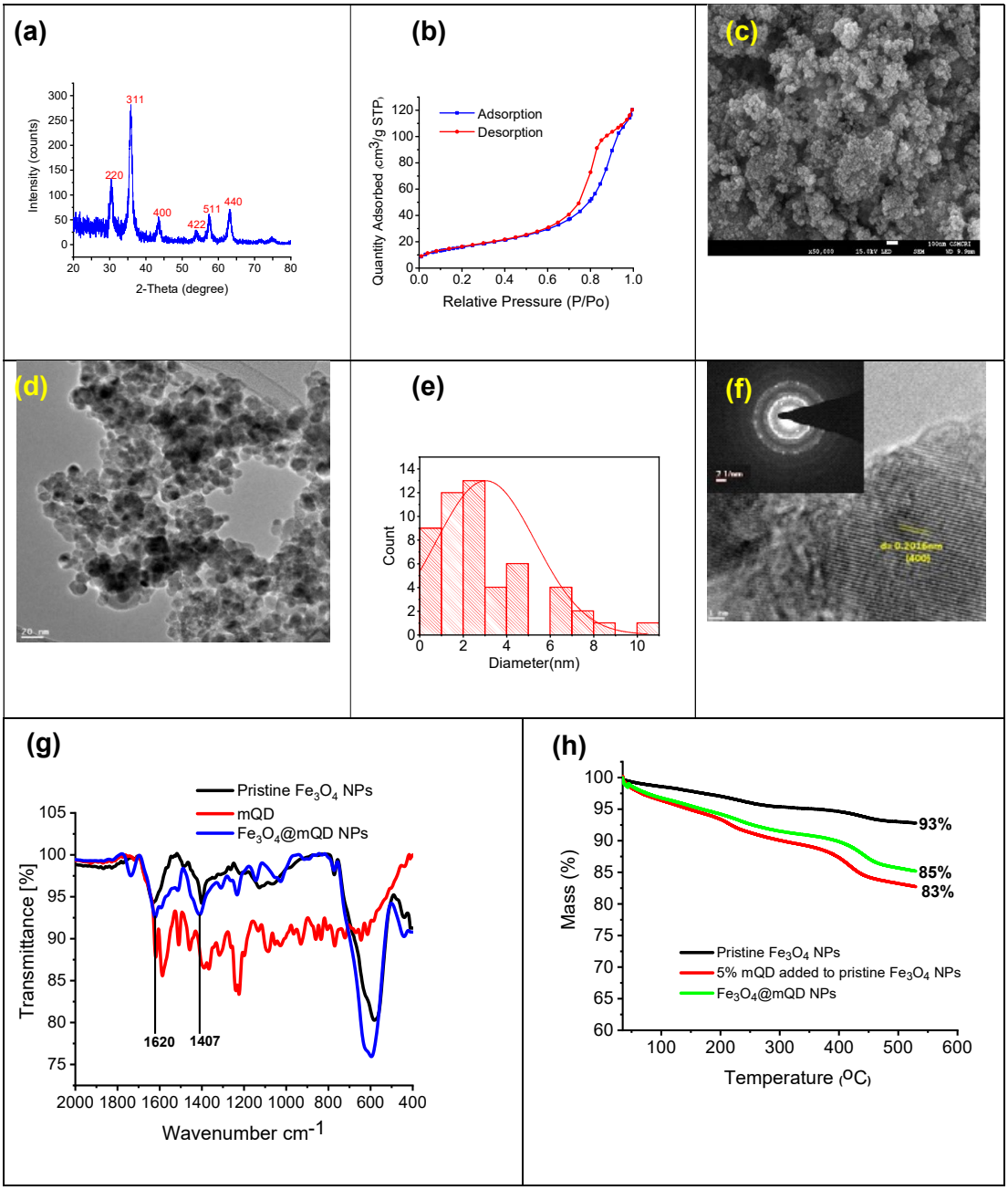

Fig. 2. (a) XRD pattern (b) nitrogen adsorption-desorption isotherms (c) SEM image (d) TEM image(e) particle size distribution (f) lattice fringes with d-spacing and SAED pattern (inset) Fe_3O_4@mQD NPs (g) FTIR spectra of pristine Fe_3O_4 NPs, free mQD and Fe_3O_4@mQD NPs (h)

TGA of the pristine Fe_3O_4 NPs, pristine Fe_3O_4 NPs spiked with 5% of mQD and Fe_3O_4 @mQD NPs

To confirm the presence of mQD on the surface of Fe_3O_4 NPs, ThermoGravimetry Analysis (TGA) was carried out. It can be observed from the thermograms that (Fig. 2h) 7.2 % weight loss occurred at 450 ^oC in the case of pristine Fe_3O_4 NPs, while that of physical mixture of 5 % mQD with pristine Fe_3O_4 NPs showed 17.3 % weight loss around 400 ^oC. When Fe_3O_4@mQD undergoes thermal degradation, 14.8 % weight loss occurred at the same temperature range. These observations indicate the chemisorption of mQD (about 6-8%) on the surface of NPs. To confirm the chirality bestowed by mQD after loading on Fe_3O_4 NPs, the synthesized Fe_3O_4@mQD NPs were dissolved in hydrochloric acid. Further, the pH of the reaction mass was adjusted to 5.5 with 1N NaOH solution. This resultant solution was evaporated to dryness, and the released mQD was extracted several times with dichloromethane and distilled, and then SOR was measured (Table 2. Fig. 3). Hence, it gets established that mQD, after loading on Fe_3O_4 NPs, retained its configuration and optical activity without any racemization or degradation.

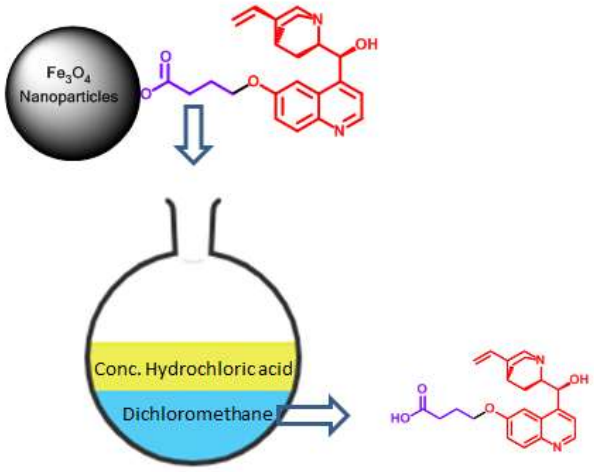

Fig. 3. Recovery process of mQD from Fe_3O_4@mQD NPs.

Table 2. Specific optical rotations (SOR) of pristine and recovered mQD.

Substrate	Specific optical rotation[a]
mQD acid (pristine)	130.40°
mQD acid (recovered)	128.03°

[a] $[\alpha]_D^{25}$ (C=1.0 Ethanol)

4.2.1 Optimization of parameters for ERO reaction

The synthesized Fe_3O_4@mQD NPs were used as a chiral Lewis base catalyst for the model ERO. For this purpose, methanolysis of anhydride **21** as a model substrate was carried out in the presence of 100 mg of Fe_3O_4@mQD NPs, and other reaction parameters were optimized. The amount of catalyst used for the model reaction can be considered 'catalytic quantity' as the amount of 'actual catalyst' (mQD) chemisorbed on the surface is less (6 -8 % from the TGA data). The reaction was performed by the treatment of the cyclic anhydride (1.0 mmol) with methanol (10.0 mol equiv.) for 60 h under the mentioned reaction conditions in diethyl ether (5.0 mL) as a solvent. The absolute configuration of the resulting chiral monoesters was determined initially by comparing their SOR ($[\alpha]_D^{25^o}$) with those reported in the literature.[38] Then the % ee of these hemiesters was determined by derivatizing it to corresponding diastereomeric amide-ester (Scheme 3 in experimental section) and injecting the reaction mixture directly to HPLC system without isolation.[15] The literature survey indicated that a good % ee could be achieved when the reaction is carried out at -40 °C or lower temperature. So the model ERO of **21** was carried out at -45°C.

4.2.2 Screening of the catalyst. The ERO of **21** was carried out in the presence of compounds obtained at various stages during the synthesis of mQD and its chemisorption on Fe_3O_4 NPs to evaluate catalytic activity and selectivity at -45 °C (Table 1). When the model reaction was carried out in the presence of a trace amount of triethylamine (TEA) as Lewis base achiral catalyst, it resulted in the mixture of racemic hemiesters (0% ee) with 100% yield within 6 h (entry 2, Table 1). The reaction hardly proceeded in a forward direction in the absence of catalyst when continued for 3 days (entry 1, Table 3). The same was also valid for model reactions when carried out in the presence of pristine Fe_3O_4 NPs at -45, 0, and 25 °C. It is necessary to note that the model reaction was not proceeded at all in the presence of free

mQD due to solubility and phase separation issues. However, when the model reaction was carried out in the presence of Fe_3O_4@mQD NPs, the % ee of the resulting product was found to be 98%. This observation confirms that the modification of the functionality at the C6' position does not hamper the catalytic activity of QD and the magnetic recovery of the catalyst is an added advantage.

Table 3. Reaction optimization in presence of different catalytic systems for enantioselective ring opening of *meso*-cyclic anhydride.[a]

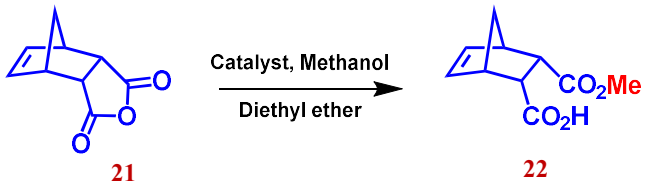

21 22

Entry	Catalyst	Yield (%)[b]	ee (%)[c]
1	None	No reaction	-
2	Triethyl amine	100	0
3	Fe_3O_4 @mQD NPs	100	98
4	Pristine Fe_3O_4	30	0
5	mQD	No reaction[d]	-

[a] The reaction was performed by treatment of the cyclic anhydride (1.0 mmol) with methanol (10.0 mmol) for 60 h, at -45°C in presence of the catalyst in diethyl ether (5.0 mL). [b] Isolated yields after column chromatography. [c]Determined by HPLC analysis of the corresponding amide derivative. [d] Reaction did not take place due to catalyst solubility and phase separation issues under the optimized reaction conditions.

4.2.3 Screening of temperature. The model ERO of *meso*-cyclic anhydride **21** was carried at 25, 0, and -45°C (Table 4). It can be observed from Table 2 that the chiral hemiester formed with 90 % and above yield, but the % ee slightly increases with a fall in temperature. The optimum selectivity was achieved (98%) at -45°C at the end of 60 h. Surprisingly, the reaction can be carried out successfully with more than 90% yield and little decrease in % ee at 25 °C within 16 h with the developed catalyst. However, all the ERO reactions are carried out at -45 °C for 60 h, in this study, without compromising the selectivity for the monoester. It is noteworthy that -45 °C was selected due to the ease of maintenance of temperature using dry-ice and acetonitrile bath under laboratory conditions.

Table 4. Effect of temperature on Fe_3O_4 @mQD NPs catalyzed enantioselective ring opening of *meso*-cyclic anhydride.[a]

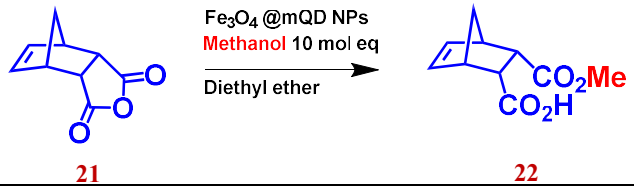

21 22

Entry	Temperature (°C)	Time (h)[d]	Yield (%)[b]	ee (%)[c]
1	**-45**	60	91	**98**
2	**0**	42	89	**96**
3	**25**	16	93	**93**

[a]The reaction was performed by treatment of **21** (1.0 mmol) with methanol (10.0 mmol) in presence of Fe_3O_4 @mQD NPs (100 mg) under the mentioned reaction conditions in diethyl ether (5.0 mL). [b]Isolated yields after column chromatography. [c]Determined by HPLC analysis of the corresponding amide derivative. [d]Maximum time required to complete the reaction, after that reaction stopped to proceed in the forward direction.

4.2.4 Screening of solvent system. The model reaction was screened for various solvents (5.0 mL) according to their order of polarity at -45°C in the presence of 100 mg Fe_3O_4@mQD NPs (Table 5). It can be observed that isopropyl alcohol is the worst solvent resulting in poor yield and a racemic mixture of hemiesters. When the model reaction was carried out in excess MeOH, acts as both, a substrate as well as a solvent, the complete conversion (100%) was achieved within 60 h with improvement in the selectivity. It can be observed that the selectivity parameters improve on shifting from polar to non-polar solvents and diethyl ether is the most suitable solvent for the purpose. It can be concluded from these experiments that the ERO should be carried out at -45 °C for 60 h in presence of a catalytic amount of Fe_3O_4@mQD NPs (100 mg) and excess MeOH (10.0 mol equiv.) in diethyl ether as a solvent to achieve the complete conversion and more than 90% ee.

Table 5. Optimization of a solvent system for Fe_3O_4@mQD NPs catalyzed enantioselective ring opening of *meso*-cyclic anhydride.[a]

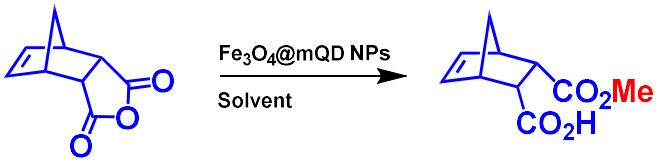

Entry	Temp (°C)	Solvent	Relative polarity	Yield (%)[b]	ee (%)[c]
1	**-45**	Methanol	5.1	97	22
2	**-45**	Diethyl ether[d]	2.8	91	98
3	**-45**	Toluene[d]	2.4	93	54
4	**-15**[e]	Carbon tetrachloride[d]	1.6	96	76
5	**-45**	Diisopropyl ether[d]	2.2	86	90
6	**-45**	Hexane[d]	0.1	78	72
7	**-45**	Tetrahydrofuran[d]	4.0	88	89
8	**-45**	Heptane[d]	0.1	81	68
9	**-40**[f]	Chlorobenzene[d]	2.7	91	92

[a]The reaction was performed by treatment of the cyclic anhydride (1.0 mmol) in the above-listed solvents (50 times of anhydride) for 60 h in the presence of Fe_3O_4 @mQD NPs (100mg). [b]Isolated yields after column chromatography. [c]Determined by HPLC analysis of the corresponding amide derivative. [d]10.0 mmole of methanol was added. [e]Below -15°C, CCl_4 begins to solidify and completely solidifies at -22.9 °C. [f]Below -40°C, chlorobenzene begins to solidify and completely solidifies at -45.6°C.

4.2.5 Screening of substrate. Anhydrides with different molecular frameworks were screened for the enantioselective methanolysis by setting the optimized parameters (Table 6). It can be observed from Table 6 that cis-3-methyl glutaric anhydride (**25**) undergoes methanolysis and yields hemiester with 93% ee under the optimized conditions. As discussed earlier, ERO protocol poorly collapsed when performed on succinic anhydrides in terms of % yield and

selectivity. Hence, succinic anhydrides with different steric were selected for ERO. This protocol is very efficient for anhydride **21** to produce hemiester **22** with almost 98% ee and complete conversion under the optimized conditions (Table 6). The selectivity slightly deteriorated when extra steric was introduced in the ring fused with an anhydride ring. Accordingly, 99% yield with 95% ee was achieved when anhydride **27** underwent ERO by MeOH, and the same is also true when the anhydride fused ring was expanded (**29**). It seems that enantioselectivity is influenced by conformational arragements and rigidity of the overall molecular framework (the more rigid structure the higher ee; for example, **29, 23** and **21**).

Table 6. Fe_3O_4 @mQD NPs - catalyzed ERO of different meso-cyclic anhydride.[a]

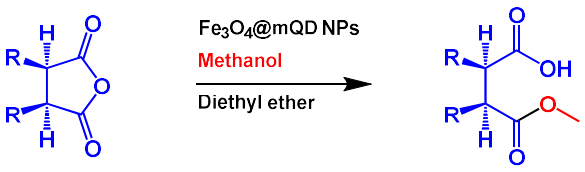

Entry	Anhydride	Products	Yield (%)[b]	ee (%)[c]
1	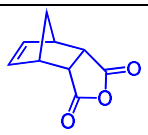	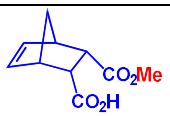	91	**98**
	21	**22**		
2	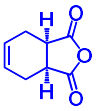	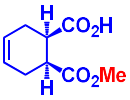	97	**93**
	23	**24**		
3	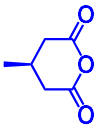	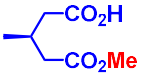	76	**93**
	25	**26**		
4	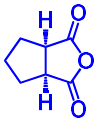	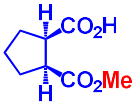	99	**95**
	27	**28**		

5	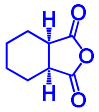	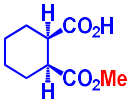	92	**96**
	29	**30**		
6	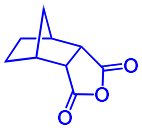	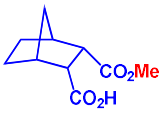	98	**96**
	31	**32**		
7		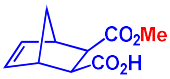	96	**98**
	33	**34**		
8		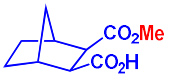	93	**96**
	35	**36**		
9	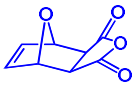	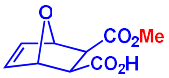	86	**97**
	37	**38**		
10	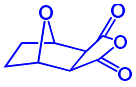	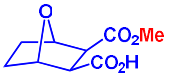	82	**97**
	39	**40**		

[a] The reaction was performed by treatment of the cyclic anhydride (1.0 mmol) with methanol (10 mmol) in the presence of Fe_3O_4 @mQD NPs (100mg) at -45°C in ether (5.0 mL). [b] Isolated yields after column chromatography. [c]Determined by HPLC analysis of the corresponding amide derivative.

It can be observed from Table 7 that almost 94% catalyst selectivity is maintained at the end of the 5th cycle of model reaction without significant loss of activity.

Table 7. Recycling of Fe_3O_4 @mQD NPs catalyst.[a]

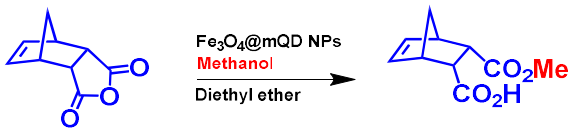

Entry	Yield (%)	ee (%)	
1	91	**98**	**1st reaction**
2	90	**97**	**3rd cycle**
3	93	**94**	**5th cycle**

[a] The reaction was performed by treatment of the cyclic anhydride (1.0 mmol) with methanol (10 mmol) in the presence of Fe_3O_4@mQD (100 mg) at -45°C in diethylether (5.0 mL). During the recycling of the catalyst there was no loss in the quantity of the catalyst observed so there was no requirement of top-up of additional catalyst.

4.2.6. Screening of the alcohols. In the next set of experiments, we carried out the ring opening reaction with exo-anhydride (**31**) and also, varying the alcohols to ensure the validity and selectivity of the developed protocol. It can be observed from the Table 8 that the protocol is effective for ERO with 1-Pentanol (**34**, 94% yield and 80% ee), while showing poor results in case of 2-Propanol (**33**) and collapsed for 2-Methyl-2-propanol. The protocol also performed good in case of aromatic alcohol like Phenylmethanol (**35**, 82% yield and 66% ee).

Table 8. Fe_3O_4 @mQD NPs - catalyzed ERO of meso-cyclic anhydride with different alcohols.[a]

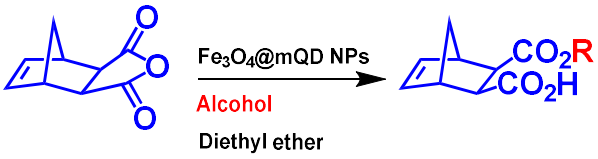

31 **32**

Entry	Alcohol	Products	Yield (%)[b]	ee (%)[c]
1	2-Propanol	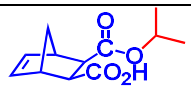	17	45

33

2	1-Pentanol	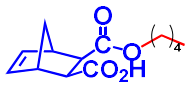 **34**	94	80
3	Phenylmethanol	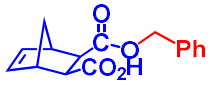 **35**	82	66
4	2-Methyl-2-propanol	-	No reaction	-

[a]The reaction was performed by treatment of the cyclic anhydride (1.0 mmol) with alcohol (10 mol equiv.) in the presence of Fe_3O_4@mQD NPs (100mg) at -45°C in ether (5.0 mL). [b]Isolated yields after column chromatography. [c]Determined by HPLC analysis of the corresponding amide derivative.

It was observed while performing the reaction that the total recovery of Fe_3O_4@mQD catalyst was possible by just applying the bar magnet at the bottom of the reaction flask, with the remaining reaction mixture contains only one of the enantiomers (~ 98%), which can be isolated by solvent distillation only and residual drying. No additional column chromatography or recrystallization is required.

4.2.7. Discussion

All through the progress in the field regarding the development of cinchona based alkaloids (CA) for the asymmetric desymmetrization of *meso*-cyclic anhydrides, mainly two strategies have been adopted (i) cinchona alkaloids and their epimers are derivatized to achieve the high selectivity and (ii) they are used as such without any modifications in their molecular framework. Though very much effective, the first approach is costly, and its application at a large scale is restricted. The major achievement in this area was the development of phenanthrene-based cinchona alkaloids modified at the C9 hydroxyl group with bulky phenanthryl group (PHN) **(36)**.[38] It was proposed that the bulky PHN group enforces the app-closed conformation of DHQD moiety. In another case, the C9 –OH group was replaced by menthol derivative (MN), resulting in the cinchona alkaloid QD-MN **(37).**[39] These modified derivatives were able to produce chiral hemiester with more than 94% ee. However, the recovery and recycling of these catalysts are challenging on a large scale.

DHQD-PHN

36

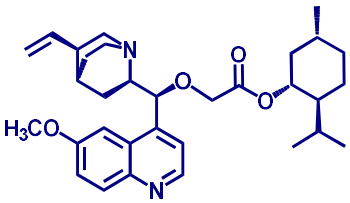

QD-MN

37

In the second approach, the natural CAs were used in the reaction without any modifications. In this case, there is a major chance of protonation of CA due to the acidic nature of the product hemiester, and the protonated CA produces racemic hemiesters that compete with non-protonated CA, deteriorating the overall selectivity. This problem was solved by adding 3^{o} amine as an additive in the reaction mixture in a stoichiometric amount.[38] Hence, from the point of view of process handling, recovery, recycling, and economics, it is worthy of anchoring the natural CA on a suitable support. However, this approach is less desired due to diffusion limitations and steric crowding around the catalyst's active sites. For example, polystyrene-supported quinine was reported as a catalyst that leads to low stereoselectivity.[40] Various siliceous materials were also used as support for CA and applied as heterogeneous catalysts for ERO.[41] They resulted in end products with up to 85% ee.

It is well established that enzymes can adopt the most suitable conformation and expose their reactive catalytic center at the interface.[42-45] The advantage of the current strategy is that it allows the free movement of quinidine and adopts the stable and active conformation at the surface. This would be resulted in a suitable enzyme-like cavity. All the active centers come into the vicinity and can orient the anhydride substrate in a proper direction (due to interactions like carbonyl dipole-dipole and CH…O) [46] such that the two carbonyl groups can be enatiotopically differentiated.[47] Due to the substrates' spatial arrangement in the catalyst's chiral environment, there is a rare chance of protonation of quinuclidine nitrogen active center (Fig. 4). Hence, maximum enantioselectivity can be obtained. With these strategies, we could achieve almost 98% ee, as can be seen in Table 6.

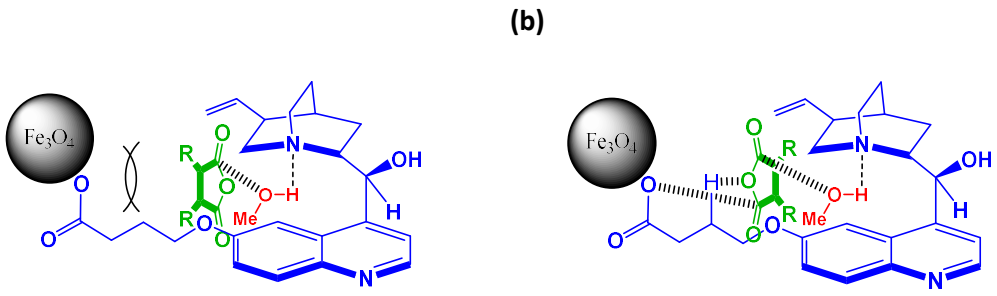

Fig. 4. Proposed different ways of spatial arrangements of *meso*-cyclic anhydride at the catalytic cavity to minimize the steric and prevent the protonation of the catalytic center. It is proposed that orientation 'b' is favored in the present case.

Now, one question that needs to be addressed is; how this mQD modified Fe_3O_4 NPs surface drives the ARO reaction to favor only one chiral hemiester? In search of the origin of high stereoselectivity, it is essential to study the surface environment and topology in detail. The molecular orientation of chiral molecules on the non-chiral magnetic surface can be probed by Uv-vis and Photoluminescence (PL) spectroscopies.

It can be observed from the UV absorption spectra that des-methyl QD (**17**) having –OH group at C6', absorbs at 340, 270, and 230 nm characteristic of quinoline moiety of the QD (Fig. 5a). These absorption bands are also designated as α, p, and β bands.[48] On substituting the –OH group with that of butyrate at C6' of QD through ether linkage (**18**) and the same with butyric acid (**19**), quench all of these three absorption bands. However, α and p bands are blue shifted in the case of Fe_3O_4@mQD (**20**), confirming the absorption on the magnetic material's surface. Interestingly, when the methanolic solution of **17** and **18** are excited at 230 nm, **17** fluoresces at 455 nm (the purple region). In comparison, the fluorescence of **18** and **19** are blue shifted to 350 nm, but **19** fluoresces with high intensity. On adsorption of mQD on Fe_3O_4 NPs surface, the emission band is red shifted at 450 nm with very high intensity (Fig. 5). This optical phenomenon indicates the rigidity of the adopted conformation of chiral mQD molecules on adsorption.[49] The ground state (S_0) and excited state (S_1) energy levels are reoriented on adsorption, favoring the radiative photoelectron transfer processes that were not possible in the case of free mQD, in a polar solvent. This observation suggests the probability of intermolecular interaction among the mQD molecules on the Fe_3O_4 NPs surface via C9 OH----N (of quinuclidine moiety) hydrogen bonding. On excitation at 230 nm, these surface adsorbed mQD molecules emit at 450 nm. This emission is 100 nm red shifted then

the free mQD molecules. This high value of red shifting indicates the collective emission from the surface adsorbed well-oriented mQD molecules.[50]

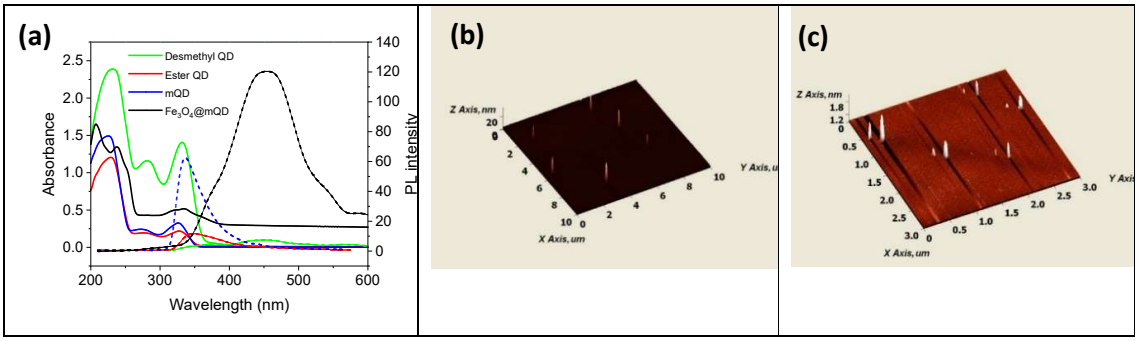

Fig. 5. (a) UV and PL spectra of as-synthesized quinidine derivatives and surface adsorbed quinidine derivative Fe_3O_4@mQD (Continuous line: UV spectra and dotted line: PL spectra) (b) AFM images of the Fe_3O_4 @ester-QD NPs (c) AFM images of the Fe_3O_4@mQD NPs.

In a special experiment to study the effect of surface adsorption on the orientation and conformation of the molecules, we synthesized Fe_3O_4 NPs by using **18** (methyl ester-QD) as a capping agent (Fe_3O_4@ester-QD) and Atomic Force Microscopy (AFM) analysis of the Fe_3O_4@ester-QD and Fe_3O_4@mQD were carried out to study the surface topology and environment. Surprisingly, we observed uniformly distributed towers on the Fe_3O_4 surface in the case of Fe_3O_4@ester-QD with about 15 nm height (Fig. 5c). In the case of Fe_3O_4@mQD, 'a pair' of uniformly distributed towers with 1.5 and 1.8 nm height could be observed. From these observations, it is confirmed that a chiral environment is created on the achiral magnetic surface. The formation of the pair of towers may be due to the suitable conformation of mQD favoring the towers' parallel growth. In contrast, in the case of Fe_3O_4@ester-QD, the proper molecular orientation could not be preferred due to the conformation, not forming the intermolecular H-bonds, which support the observations of chiroptical analysis. However, we cannot predict more about magnetic chiral surface growth due to the limitations of growing the Fe_3O_4 single crystals and further research is required in this direction.

To demonstrate the application of the as-synthesized Fe_3O_4@mQD NPs for ERO by methanolysis, we carried out the reaction in a mini-pilot plant. The flow diagram of the unit processes carried out for the production of chiral hemiester starting from 0.1 mol of

anhydride **21** is shown in Fig. 6. It is noteworthy from the Fig. 4 that there are two reactors used for the production of hemiester. In Reactor-1 all the reagents, solvent and the catalyst were mixed according to the optimized stoichiometric ratio and the reaction temperature (-45 ^{o}C) was maintained by circulating the solution of dry ice in acetonitrile in the jacket. After completion of the reaction in the stipulated time, the mixture was allowed to settle and the catalyst particles are sticked on the surface of the magnetic needle (black needle in Fig. 6). Then the reaction mixture was transferred to the Reactor-2 for solvent recovery by circulating the hot water in the jacket surround the reactor and the product was separated from the bottom. The recoverd solvent was cooled by circulating the brine solution, stored and recycled for the next reaction cycle.

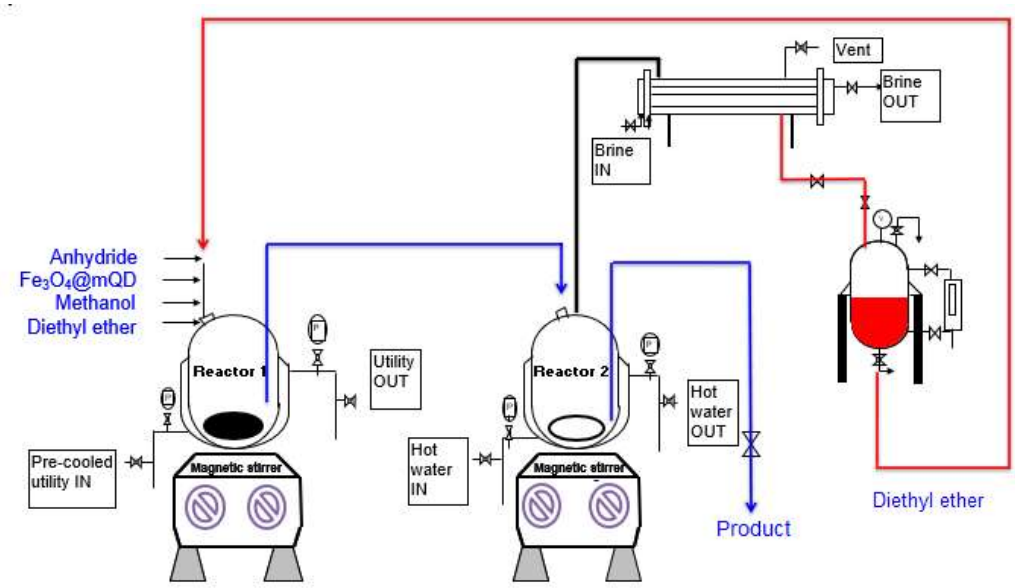

Fig. 6. Flow diagram for the pilot-scale enantioselective ring opening of *meso*-cyclic anhydrides by methanolysis in presence of Fe_3O_4@mQD NPs.

The product monoester was formed with 93% molar yield and 98% ee. The procedure adopted for the production of the target material in a mini-pilot plant is discussed in detail in the experimental section.

4.3. Experimental

All the chemicals were purchased from Aldrich Chemicals unless specified. $FeCl_3 \cdot 6H_2O$ was purchased from Loba Chemie, India. $FeSO_4 \cdot 4H_2O$ was purchased from S. D. Fine Chemicals

Limited, India. Aqueous ammonia was purchased from S. R. Enterprise, India. Des-methyl quinidine was gifted from Dr. Nagar's Laboratories, Vadodara, Gujarat, India. An X-ray powder diffraction (XRD) pattern was obtained using an X-ray powder diffractometer (Philips X'pert MPD system) with Cu Kα radiation, λ = 0.15418 nm. The BET specific surface area (SBET) was determined by nitrogen adsorption (Micrometrics ASAP 2020, USA) via a multipoint BET method using the adsorption data in the relative pressure (P/P^o) range of 0.0–1.0. The samples were degassed at 80 ^oC prior to Brunauer–Emmett–Teller (BET) measurements. Desorption isotherm was used to determine the pore-size distribution using the Barret–Joyner–Halendar (BJH) method, assuming a cylindrical pore model. The nitrogen adsorption volume at the relative pressure (P/P^o) range of 0.997 was used to determine the pore volume and average pore size. The morphology of the samples was examined by FESEM (JEOL-JSM-7100F). Particle size with elemental mapping was carried out by TEM (JEOL-JEM-2100) at 200 kV. FT-IR spectra of all compounds were recorded with Bruker FTIR spectrometer using KBr pallets in the range of 400 to 4000 cm^{-1}. Optical rotations were measured on JACSO P-2000 polarimeter and HPLC analyses were carried out on Jasco HPLC system at 280nm. AFM analysis was carried out on NT-MDT, Ntegra Aura and CD spectra on JASCO, J-815. UV– visible absorption spectra were recorded on a Perkin Elmer Lambda 35 and PL spectra were recorded on a Jasco FP-6300 spectrophotometer using Xenon lamp as an excitation source at 280 nm. All measurements were made at 25 ^oC in methanol. HRMS was recorded on Xevo G2-S Q Tof (Waters, USA), TG analysis were recorded on Exstar TG/DTA7000 from 30 to 550 ^oC with heating rate of 10 ^oC. The sample size was between 2-8mg. The ^1H NMR and ^{13}C NMR were recorded on a Bruker Avance 300 and 75 MHz spectrometer using TMS as an internal standard in $CDCl_3$.

4.3.1 Synthesis of 4-((4-((1S)-hydroxy((2R,4S,5R)-5-vinyl quinuclidin-2-yl)methyl)quinolin-6-yl)oxy)butanoic acid methyl ester (18).

In 45 mL DMSO, 0.723 g KOH (12.88 mmol, 2 equiv.) was dissolved and stirred at 500 rpm. After 10 min, 2.0 g desmethyl quinidine (6.44 mmol, 1 equiv.) was added in the above solution, and the mixture was maintained at RT under N_2 atmosphere for 6 h. After the change of color of the solution to dark brown, 3.5 g methyl bromobutyrate (19.33 mmol, 3.0 equiv.) was added, and the mixture was stirred at RT for 20 h. Then it was treated with water (450

mL) and extracted thrice with CH_2Cl_2 (100 mL); the organic layer was then washed three times with H_2O (100 mL), and dried on anhydrous Na_2SO_4. The solvent was evaporated and the residue was purified by silica gel chromatography EtOAc:Et_3N:MeOH, 50:1:2 to afford pure ester **18** (83.3% yield). ^{1}H NMR (300 MHz, DMSO-d6) δ 8.68 (d, J=4.2 Hz, 1H), 7.93 (d, J=9.0Hz, 1H), 7.50 (d, J=4.2 Hz, 1H), 7.37 (dd, J=9.0, 2.7 Hz, 1H), 7.49 (d, J=2.4 Hz, 1H), 5.88 (ddd, J= 17.1, 9.0, 2.7Hz, 1H), 5.62 (d, J= 4.5 Hz1H), 5.4 (t, J=5.4 Hz, 1H), 4.93-5.02 (m, 2H), 4.19-4.10 (m, 2H), 3.62 (s, 3H), 3.16 (m, 1H), 3.06 (q, J=7.8 Hz, 1H), 2.85 (dd, J=13.5, 3.3Hz, 1H), 2.39-2.57 (m, 4H), 2.19(m, 1H), 2.07 (quin, J=7 Hz, 2H), 1.59-1.77 (m, 4H), 1.42 (m, 1H); ^{13}C NMR(75 MHz, DMSO-d6) δ 24.57, 27.94, 30.45, 40.05, 42.23, 51.81, 56.36, 61.10, 67.29, 71.47, 103.75, 114.50, 119.62, 121.58, 127.54, 131.64, 143.03, 144.40, 147.98, 149.71, 156.38, 173.48. FTIR (cm^{-1}) 3431, 379, 2942, 2870, 1737, 1620, 1590, 1509, 1451, 1362, 1322, 1238, 1197, 1170, 1135, 1097, 1045, 998, 961, 912, 856, 826. HRMS (ESI) m/z $(M+H)^+$ calculated for 411.2283, observed: 411.2284. $[\alpha]_D^{25}$ +128.03° (C=1.0 Ethanol)

4.3.2 Synthesis of 4-((4-((1S)-hydroxy((2R,4S,5R)-5-vinylquinuclidin-2-yl)methyl)quinolin-6-yl)oxy)butanoic acid (mQD) (19).

1.00 g of methyl ester (**18**) (2.43 mmol, 1 equiv.) was dissolved in 20 mL KOH solution (1.77 g, 31.67 mmol, 13 equiv.) in absolute ethanol. The mixture was maintained at RT overnight and concentrated in a vacuum. The residue was treated with H_2O (20 mL), acidified with HCl (2.0 N) to pH 5.5, and evaporated. The residue was then treated three times with CH_2Cl_2 (100 mL) and dried over anhydrous Na_2SO_4. The solvent was removed under reduced pressure resulting in **19**.

^{1}H NMR (300MHz, DMSO-d6) δ 8.72 (d, J=4.5 Hz, 1H), 7.98 (d, J= 1.8, 1H), 7.93 d, J=9, 1H), 7.59 (d, J=4.5, 1H), 7.35 (dd, J=2.4, 9.3, 1H), 6.14 (brs, 1H), 5.88 (s, 1H), 5.80 (ddd, J= 17.1, 9.0, 2.4Hz, 1H), 5.03 (d, J=17.1, 1H), 4.94 (d, J=10.5, 1H), 4.24 (m, 2H), 3.71 (m, 1H), 3.29-3.41 (m,2H), 2.79-2.94 (m, 2H), 2.56 (m, 1H), 2.26-2.31 (m, 2H), 1.72-2.05 (m, 6H), 1.47 (m, 1H); ^{13}C NMR (75 MHz, DMSO-d6) δ 18.74, 24,16, 25.19, 27.57, 32.42, 38.07, 42.07, 53.81, 59.35, 67.14, 68.68, 102.61, 115.98, 119.18, 122.7, 126.55, 131.63, 140.54, 144.00, 147.34, 147.81, 157.40, 176.08. FTIR (cm^{-1}) 3422, 2946, 2875, 2378, 2307, 1618, 1586, 1509, 1457, 1366, 1316,

1223, 1085, 1027, 930, 859, 834, 769, 721, 669. HRMS (ESI) m/z $(M+H)^+$ calculated for 397.2127, observed: 397.2127. $[\alpha]_D^{25}$ +130.40° (C=1.0 Ethanol).

4.3.3 Supporting 4-((4-((1S)-hydroxy((2R,4S,5R)-5-vinylquinuclidin-2-yl)methyl)quinolin-6-yl)oxy)butanoic acid on *in situ* generated Fe_3O_4 magnetic nanoparticles (Fe_3O_4 @mQD NPs) (20).

Modified quinidine m(QD) derivative coated magnetite nanoparticles were synthesized by the one-pot synthesis method. In brief, ferric chloride (1.42 g, 8.7 mmol) and ferrous chloride tetrahydrate (1.00 g, 5.02 mmol), molar ratio 1.75:1, respectively were added to 50 mL deionized water in an inert atmosphere. The mixture was heated to 70 °C to obtain a clear yellow solution. The mixture was stirred vigorously with a mechanical stirrer to avoid interparticle magnetic interaction. After 30 min, modified quinidine (mQD) (7.97 g, 20.1 mmol), dissolved in deionized water (25 mL) was rapidly added. The solution was further cleared by the addition of conc. HCl (7 mL) and stirred for another 30 min. Then 20 mL ammonia solution (about 25% in water) was rapidly added. The reaction color was changed to black. The stirring was continued for 1.5 h. Finally, the black nanoparticles were separated magnetically, washed with distilled water (200 mL) three times, and washed with methanol (200 mL) three times, then dried in an oven at 100 °C overnight. Dry weight of nanoparticles: 1.2 g

4.3.4 General procedure for Fe_3O_4@mQD NPs mediated ring opening of *meso*-cyclic anhydride.

Methanol (10.0 mmol) was added dropwise to a stirred suspension of the anhydride (1.0 mmol) and the Fe_3O_4 @mQD NPs (100 mg) in diethyl ether (5.0 mL) at -45 °C under argon. The reaction mixture was stirred at this temperature for 60 h. During this period, the anhydride gradually dissolved. Subsequently, the catalyst is separated by applying a magnet and the resulting clear solution was concentrated *in vacuo* to dryness, resulting in the corresponding monoester.

(a) **(b)**

Fig. 7. (a) Reaction mixture of Anhydride, Methanol and Fe_3O_4@mQD NPs under stirring with magnetic bar (**b)** reaction mixture when magnetic stirring is stopped and the catalyst sticks to the magnetic needle.

4.3.5. Determination of diastereomeric excess

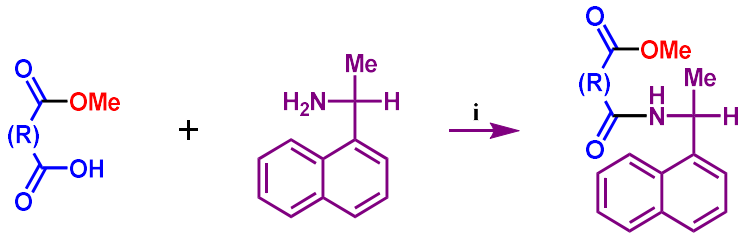

Scheme 3. Reagents and conditions: i. $SOCl_2$, NEt_3, dry toluene, 0°C 1h. [15]

Diastereomeric excess was determined by adopting the procedure developed by Hiratake et al. [15]. A representative procedure is as follows (Scheme 3). Thionyl chloride (1.95 mmol) was added to a solution of the monoester (1.5 mmol) in dry toluene (25.0 mL) at 0 °C. The mixture was stirred at 0 °C for 10 min, and then (R)-1-(1-naphthy1)ethylamine (1.8 mmol) and triethylamine (5.25 mmol) were added successively. The mixture was stirred at 0 °C for 1 h, then at room temperature for an additional 1 h. The solvent was removed under reduced pressure and the residue was dissolved in ethyl acetate (200 mL). The solution was washed successively with 50 mL of 1M HCl, saturated aq. $NaHCO_3$ and saturated aq. NaCl. The organic layer was dried (Na_2SO_4) and evaporated to give a diastereomeric mixture.

(1S,2R,3S,4R)-3-(methoxycarbonyl)bicyclo[2.2.1]hept-5-ene-2-carboxylic acid (22) was obtained from the Fe_3O_4@mQD NPs catalyzed methanolysis of anhydride in 91% yield as a white solid and in 98% ee as determined by HPLC analysis of the diastereomeric mixture of the corresponding amide-ester prepared as described above (Hypersil, 20:1, hexanes:IPA, 0.5 mL/min), t(major)= 18.09 min., t(minor)= 14.81 min.); $[\alpha]_D^{25}$ (+7.2 (*c* =4.23, CCl_4), literature [29]: $[\alpha]_D^{25}$ +7.8 (*c* =4.23, CCl_4) % for ee: 99%; ^{1}H NMR (300 MHz, $CDCl_3$): δ 1.33 (bd, J=9.0 Hz,1H), 1.50 (dt, J=9.0 Hz and J=1.8 Hz, 1H), 3.16-3.36 (m, 4H), 3.59 (s, 3H), 6.22 (dd, J=5.0 and 3.0 Hz, 1H) 6.26 (dd J=5.0 and 3.0 Hz, 1H), 6.23 (br s, 1H). ^{13}C NMR (75 MHz, $CDCl_3$): δ 46.30, 46.58, 48.00, 48.26, 48.79, 51.53, 134.34, 135.57, 172.96, 177.97.

(1R,6S)-6-(methoxycarbonyl)cyclohex-3-ene-1-carboxylic acid (24) was obtained from the Fe_3O_4@mQD NPs catalyzed methanolysis of anhydride in 97% yield as a colourless oil and in 96% ee as determined by HPLC analysis of the diastereomeric mixture of the corresponding amide-ester prepared as described above (Hypersil, 20:1, Hexanes:IPA, 0.5 mL/min, t(major)=10.83 min., t(minor)=9.23 min.); ^{1}H NMR (300 MHz, $CDCl_3$): δ 2.32- 2.41 (m, 2H), 2.54-2.63 (m, 2H), 3.03-3.11 (m, 2H), 3.70 (s, 3H), 5.68 (AB-system, *J* = 1.7 Hz, 2H), 7.62 (br s, 1H). ^{13}C NMR (75 MHz, $CDCl_3$): δ 25.55, 25.73, 39.48, 39.59, 51.95, 125.06, 125.15, 173.77, 179.39.

(S)-5-methoxy-3-methyl-5-oxopentanoic acid (26) was obtained from the Fe_3O_4@mQD NPs catalyzed methanolysis of anhydride in 76% yield as a colourless oil and in 93% ee as determined by HPLC analysis of the diastereomeric mixture of the corresponding amide-ester prepared as described above (Hypersil, 20:1, hexanes:IPA, 0.5 mL/min, t(major)=7.45 min., t(minor)=6.64 min.); ^{1}H NMR (300MHz, $CDCl_3$): δ 0.98 (d, J = 6.0 Hz, 3H), 2.17-2.44 (m, 5H), 3.61(s, 3H); ^{13}C NMR (75 MHz, $CDCl_3$) δ 19.82, 27.17, 40.50, 40.51, 51.58, 172.94, 178.28.

(1R,2S)-2-(methoxycarbonyl)cyclopentane-1-carboxylic acid (28) was obtained from the Fe_3O_4 @mQD NPs catalyzed methanolysis of anhydride in 99% yield as a colourless oil and in 95% ee as determined by HPLC analysis of the diastereomeric mixture of the corresponding amide-ester prepared as described above (Hypersil, 20:1, hexanes:IPA, 0.5 ml/min, t(major)=13.13 min., t(minor)=10.91 min.); ^{1}H NMR (300 MHz, $CDCl_3$): δ 1.60-1.72 (m, 1H), 1.83-2.11 (m, 5H), 3.03-3.13 (m, 2H), 3.66 (s, 3H), 6.66 (br s, 1H). ^{13}C NMR (75 MHz, $CDCl_3$): δ 23.83, 28.68, 46.80, 46.85, 51.79, 174.45, 180.11.

(1R,2S)-2-(methoxycarbonyl)cyclohexane-1-carboxylic acid (30) was obtained from the Fe_3O_4 @mQD NPs catalyzed methanolysis of anhydride in 92% yield as white foam and in 93% ee as determined by HPLC analysis of the diastereomeric mixture of the corresponding amide-ester prepared as described above (Hypersil 20:1, hexanes:IPA, 0.5 ml/min, t(major)=11.38 min., t(minor)=9.33 min.); ^{1}H NMR (300 MHz, CDCl3): δ 1.46-1.58 (m, 4H), 1.74-1.82 (m, 2H), 1.98-2.06 (m, 2H), 2.84-2.85 (m, 2H), 3.69 (s, 3H), 10.39 (br s, 1H). ^{13}C NMR (75 MHz, CDCl3): δ 23.64, 23.76, 25.95, 26.26, 42.33, 42.54, 51.74, 174.10, 180.20.

(1R,2R,3S,4S)-3-(methoxycarbonyl)bicyclo[2.2.1]heptane-2-carboxylic acid (32) was obtained from the Fe_3O_4 @mQD NPs opening of anhydride in 98% yield as white foam and in **96.00** % ee as determined by HPLC analysis of the diastereomeric mixture of the corresponding amide-ester prepared as described above (Hypersil 20:1, hexanes:IPA, 0.5 ml/min, t(major)=33.69 min., t(minor)=32.01 min.); ^{1}H NMR (300 MHz, $CDCl_3$): δ 1.45-1.48 (m, 4H), 1.79-1.81 (m, 2H), 2.56-2.59 (m, 2H), 2.96-3.06 (m, 2H), 3.64 (s, 3H), 9.91 (br s, 1H); ^{13}C NMR (75 MHz, $CDCl_3$): δ 23.89, 24.07, 39.87, 40.14, 40.43, 46.75, 51.32, 172.88, 178.78.

(1R,2R,3S,4S)-3-(methoxycarbonyl)bicyclo[2.2.1]heptane-2-carboxylic acid (34) was obtained from the Fe_3O_4 @mQD NPs opening of anhydride in 96% yield as white solid and in **98.20** % ee as determined by HPLC analysis of the diastereomeric mixture of the corresponding amide-ester prepared as described above (Hypersil 20:1, hexanes:IPA, 0.5 ml/min, t(major)=17.06 min., t(minor)=15.48 min.); ^{1}H NMR (300 MHz, $CDCl_3$): δ 1.50 (bd, 1H), 2.10 (bd, 1H), 2.65 (m, 2H), 3.12 (m, 2H), 3.66 (s, 3H), 6.22 (m, 2H), 9.40 (bs, 1H). ^{13}C NMR (75 MHz, $CDCl_3$): δ 45.38, 45.42, 45.78, 47.40, 47.45, 51.84, 137.91, 138.06, 173.96, 179.83.

(1R,2R,3S,4S)-3-(methoxycarbonyl)bicyclo[2.2.1]heptane-2-carboxylic acid (36) was obtained from the Fe_3O_4 @mQD NPs opening of anhydride in 93% yield as light yellow foam and in **96.40** % ee as determined by HPLC analysis of the diastereomeric mixture of the corresponding amide-ester prepared as described above (Hypersil 20:1, hexanes:IPA, 0.5 ml/min, t(major)=26.95 min., t(minor)=25.26 min.); ^{1}H NMR (300 MHz, $CDCl_3$): δ 1.24-1.29 (m, 3H), 1.58-1.65 (m, 2H), 2.02-2.05 (m, 1H), 2.59 (s, 2H), 2.73-2.77 (m, 2H), 3.63 (s, 3H), 8.26 (br s, 1H); ^{13}C NMR (75 MHz, $CDCl_3$): δ 28.63, 28.80, 35.78, 39.72, 40.14, 50.88, 50.92, 51.58, 173.49, 179.26.

(1S,2R,4R)-3-(methoxycarbonyl)-7-oxabicyclo[2.2.1]hept-5-ene-2-carboxylic acid (38) was obtained from the Fe_3O_4 @mQD NPs opening of anhydride in 86% yield as off white foam and in **97.28** % ee as determined by HPLC analysis of the diastereomeric mixture of the corresponding amide-ester prepared as described above (Hypersil 20:1, hexanes:IPA, 0.5 ml/min, t(major)=27.18 min., t(minor)=25.52 min.); ^{1}H NMR (300 MHz, $CDCl_3$): δ 2.82-2.87 (m, 2H), 3.69 (s, 3H), 5.27 (m, 1H), 5.33 (m, 1H), 6.46 (m, 2H), 7.49 (br s, 1H). ^{13}C NMR (75 MHz, $CDCl_3$): δ 46.09, 46.91, 52.35, 79.9, 80.45, 136.48, 136.69, 172.09, 176.44.

(1S,2R,4R)-3-(methoxycarbonyl)-7-oxabicyclo[2.2.1]heptane-2-carboxylic acid (40) was obtained from the Fe_3O_4 @mQD NPs opening of anhydride in 82% yield as yellow solid and in **97.04** % ee as determined by HPLC analysis of the diastereomeric mixture of the corresponding amide-ester prepared as described above (Hypersil 20:1, hexanes:IPA, 0.5 ml/min, t(major)=26.83 min., t(minor)=26.00 min.); ^{1}H NMR (300 MHz, CDCl3): δ 1.52-1.58 (m, 2H), 1.80-1.89 (m, 2H), 3.01-3.06 (m, 2H), 3.67 (s, 3H), 4.91-4.92 (m, 1H), 4.97-4.98 (m, 1H), 6.77 (br s, 1H). ^{13}C NMR (75 MHz, CDCl3): δ 28.97, 28.99, 52.14, 52.26, 52.29, 78.33, 78.62, 171.38, 176.25.

(1S,2S,4R)-3-((pentyloxy)carbonyl)bicyclo[2.2.1]hept-5-ene-2-carboxylic acid (34) was obtained from the Fe_3O_4 @mQD NPs catalyzed alcoholysis of anhydride with 1-pentanol in 94% yield as white solid and in **82** % ee as determined by HPLC analysis of the diastereomeric mixture of the corresponding amide-ester prepared as described above (Hypersil 25:1, hexanes:IPA, 0.5 ml/min, t(major)=15.7 min., t(minor)=14.2 min.); ^{1}H NMR (500 MHz, $CDCl_3$): δ 0.91 (t, 3H), 1.32-1.36 (m, 4H), 1.5 (d, 1H), 1.61 (m, 2H), 2.12 (d, 1H), 2.64 (t, 1H), 3.12 (s, 1H), 3.9-4.1(m, 2H), 6.22 (s, 2H), 9.61 (br s, 1H). ^{13}C NMR (125 MHz, $CDCl_3$): δ 13.97, 22.31, 28.06, 28.16, 45.38, 45.49, 45.78, 47.32, 47.60, 65.03, 137.84, 138.15, 173.43, 179.91.

(1S,2S,4R)-3-((benzyloxy)carbonyl)bicyclo[2.2.1]hept-5-ene-2-carboxylic acid (35) was obtained from the Fe_3O_4 @mQD NPs catalyzed alcoholysis of anhydride with phenylmethanol in 82% yield as white solid and in **65**% ee as determined by HPLC analysis of the diastereomeric mixture of the corresponding amide-ester prepared as described above (Hypersil 25:1, hexanes: IPA, 0.5 mL/min, t(major)=19.0 min., t(minor)=17.8 min.); ^{1}H NMR (500 MHz, $CDCl_3$): δ 1.52-1.55 (m, 1H), 2.16 (d, 1H), 2.66-2.73 (d, 2H), 3.13-3.17 (d, 2H), 5.02-5.17 (m, 2H), 6.24 (t, 2H), 7.28-7.39 (m, 5H), 10.05 (br s, 1H). ^{13}C NMR (125 MHz, $CDCl_3$): δ 45.42, 45.56, 45.86, 47.45, 47.54, 66.77, 128.21, 128.33, 128.56, 135.78, 137.94, 138.10, 173.29, 179.93.

4.3.6. Production of hemiester (22) in the mini-pilot plant. Methanol (32.0 g) was added dropwise to a stirred suspension of cis-5-norbornene-endo-2,3-dicarboxylic anhydride (16.4 g) and the Fe_3O_4 @mQD NPs (10.0 g) in diethyl ether (5000 mL) at -45 °C under argon. The reaction mixture was stirred at this temperature for 60 h. During this period, the anhydride gradually dissolved. After completion of the reaction, the mass is transferred to another reactor enabling the separation of the catalyst magnetically. The clear solution was distilled by applying hot water of 60-65^{o}C. After completion of the distillation the corresponding monoester 18.2g, (93% molar yield, 98% ee) was isolated from the bottom of the reactor as oil which solidified as white solid upon storage. The recovered ether was 3600 mL and 99.0% purity by GC and was having moisture less than 0.1%. It was suitable for use for the next reaction without further purification.

4.3.7. Characterization

X-ray powder diffraction (XRD) pattern was obtained using an X-ray powder diffractometer (Philips X'pert MPD system) with Cu Kα radiation, λ = 0.15418 nm. The BET specific surface area (SBET) was determined by nitrogen adsorption (Micrometrics ASAP 2020, USA) via a multipoint BET method using the adsorption data in the relative pressure (P/P^{o}) range of 0.0–1.0. The samples were degassed at 80 ^{o}C before Brunauer–Emmett–Teller (BET) measurements. Desorption isotherm was used to determine the pore-size distribution using the Barret– Joyner–Halendar (BJH) method, assuming a cylindrical pore model. The nitrogen adsorption volume at the relative pressure (P/P^{o}) range of 0.997 was used to determine the pore volume and average pore size. The morphology of the samples was examined by FESEM (JEOL-JSM-7100F). Particle size with elemental mapping was carried out by TEM (JEOL-JEM-2100) at 200 kV. FT-IR spectra of all compounds were recorded with Bruker FTIR spectrometer using KBr pellets in the range of 400 to 4000 cm^{-1}. Optical rotations were measured on the JACSO P-2000 polarimeter and HPLC analyses were carried out on the JASCO HPLC system at 280nm. AFM analysis was carried out on NT-MDT, Ntegra Aura, and CD spectra on JASCO, J-815. UV– visible absorption spectra were recorded on a Perkin Elmer Lambda 35 and PL spectra were recorded on a JASCO FP-6300 spectrophotometer using a Xenon lamp as an excitation source at 280 nm. All measurements were made at 25 ^{o}C in methanol. HRMS was recorded on Xevo G2-S Q Tof (Waters, USA), TG analysis was recorded on Exstar TG/DTA7000 from 30 to 550 ^{o}C with a heating rate of 10 ^{o}C. The sample size was between 2-8 mg. The ^{1}H

NMR and ^{13}C NMR were recorded on a Bruker Avance 300, 500, 125 and 75 MHz spectrometer using TMS as an internal standard in DMSO-d6 and $CDCl_3$. All the spectra are reported in ESI.

HPLC chromatograms and NMR spectra of the products and mQD intermediates:

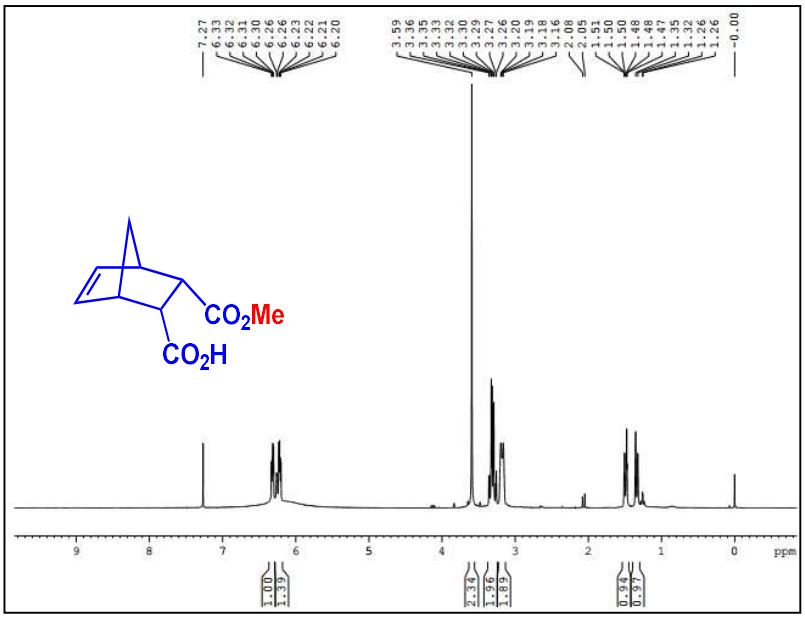

Fig. 8. ^{1}H NMR of (2*R*, 3*S*)-3-*endo*-Methoxycarbonyl-bicyclo[2.2.1]hept-5-ene-2-*endo*-carboxylic acid.

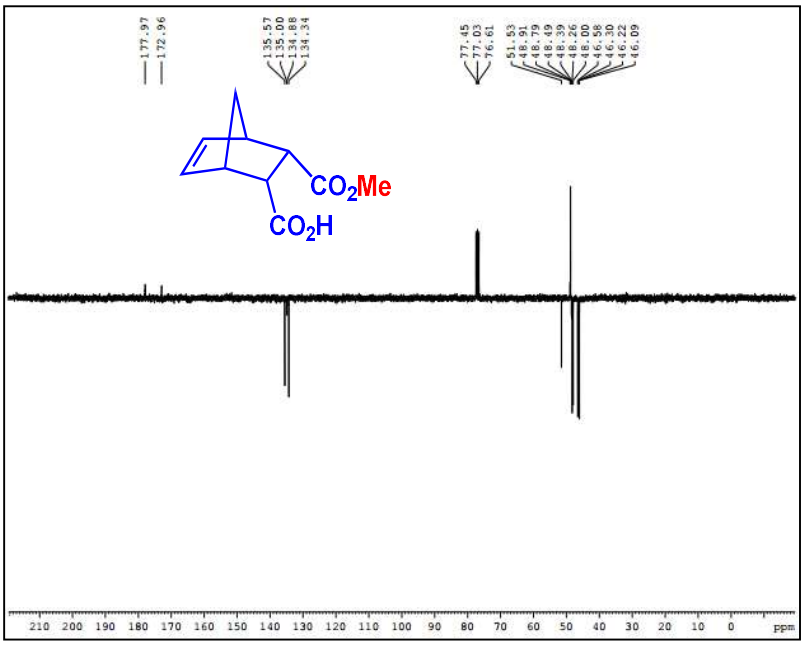

Fig. 9. ^{13}C NMR of (2*R*, 3*S*)-3-*endo*-Methoxycarbonyl-bicyclo[2.2.1]hept-5-ene-2-*endo*-carboxylic acid.

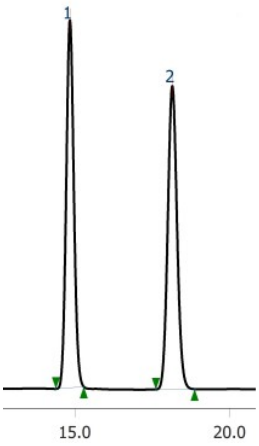

	Retention time	Area	Area %
1	14.837	9732165	49.816
2	18.140	9804210	50.184

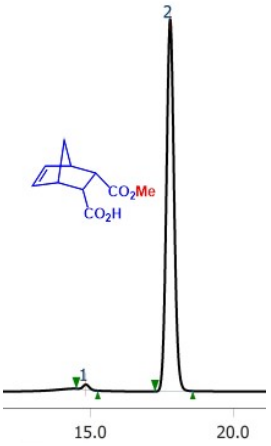

	Retention time	Area	Area %
1	14.819	142127	1.125
2	18.098	12491520	98.875

Fig. 10. HPLC chromatograms of racemic and (2*R*, 3*S*)-3-*endo*-Methoxycarbonyl-bicyclo[2.2.1]hept-5-ene-2-*endo*-carboxylic acid.

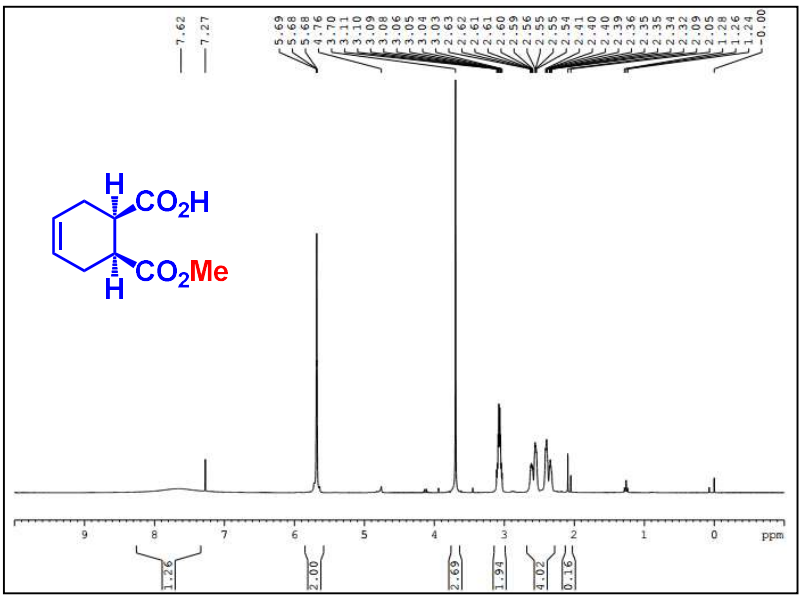

Fig. 11. ^{1}H NMR of (1*R*,2*S*)-*cis*-2-Methoxycarbonyl-cyclohex-4-ene-1-carboxylic acid.

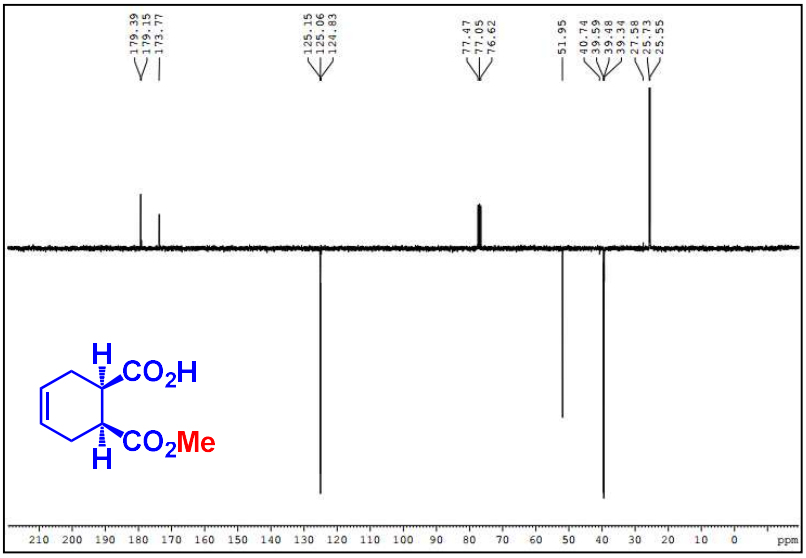

Fig. 12. ^{13}C NMR of (1*R*, 2*S*)-*cis*-2-Methoxycarbonyl-cyclohex-4-ene-1-carboxylic acid.

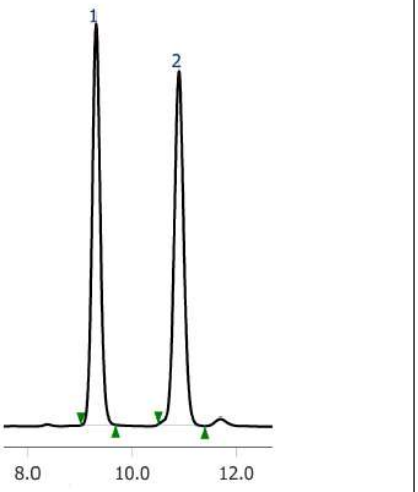

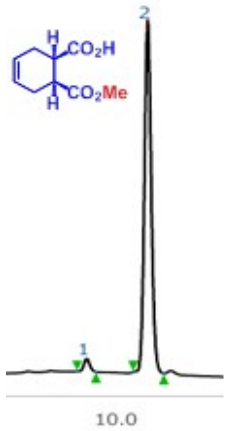

	Retention time	Area	Area %
1	9.297	12616616	49.118
2	10.890	13069550	50.882

	Retention time	Area	Area %
1	9.233	230010	1.872
2	10.830	12056858	98.128

Fig. 13. HPLC chromatographs of racemic and (1*R*, 2*S*) *cis*-2-Methoxycarbonyl-cyclohex-4-ene-1-carboxylic acid.

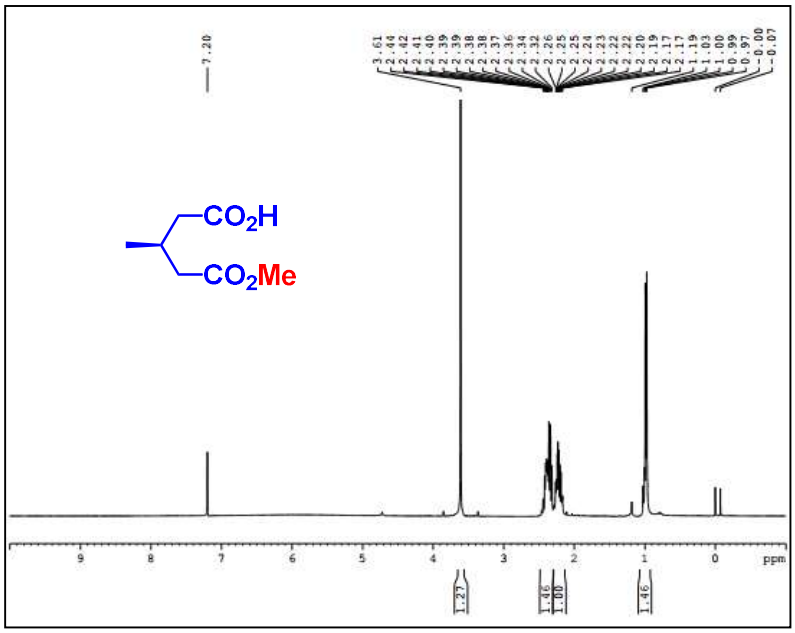

Fig. 14. ^{1}H NMR of (3R)-5-methoxy-3-methyl-5-oxopentanoic acid.

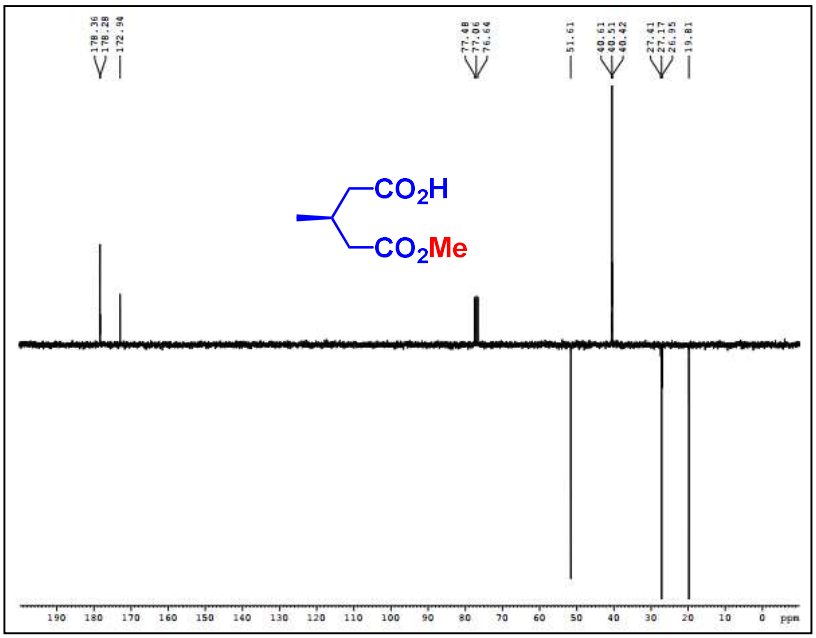

Fig. 15. ^{13}C NMR of (3R)-5-methoxy-3-methyl-5-oxopentanoic acid.

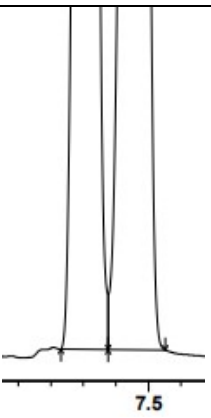

	Retention time	Area	Area %
1	6.631	7946040	49.274
2	7.406	8180067	50.726

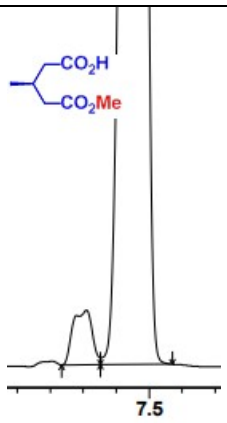

	Retention time	Area	Area %
1	6.647	558829	3.600
2	7.459	14965172	96.400

Fig. 16. HPLC chromatograms of racemic and (3R)-5-methoxy-3-methyl-5-oxopentanoic acid.

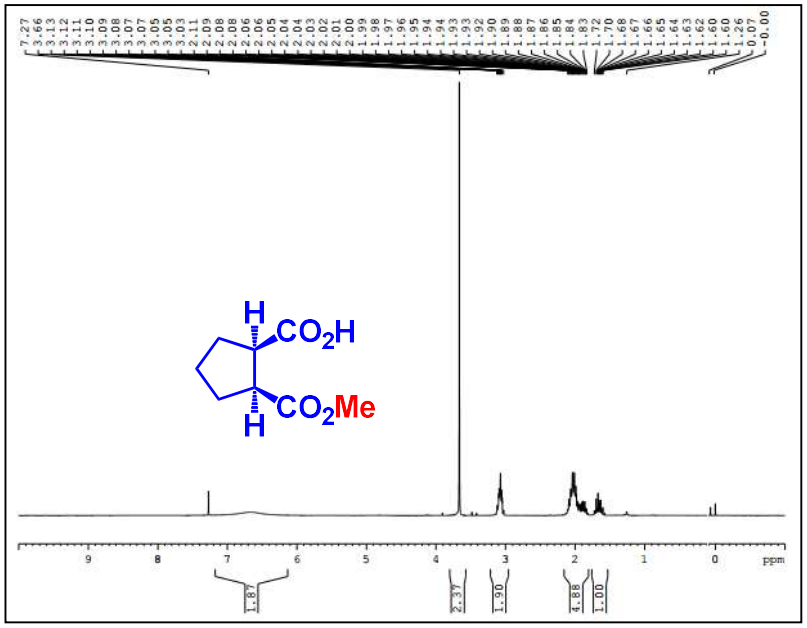

Fig. 17. ^{1}H NMR of (1*R*,2*S*)-*cis*-2-Methoxycarbonyl-cyclopentane-1-carboxylic acid.

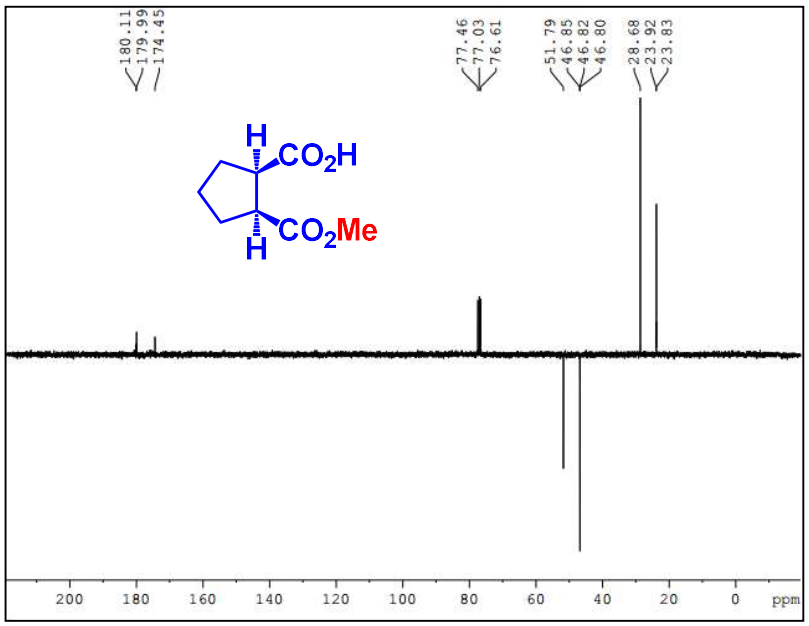

Fig. 18. ^{13}C NMR of (1*R*, 2*S*)-*cis*-2-Methoxycarbonyl-cyclopentane-1-carboxylic acid.

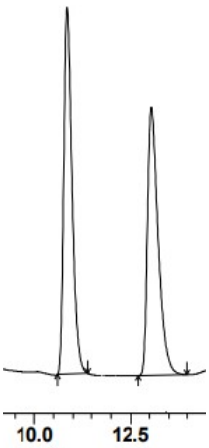

	Retention time	Area	Area %
1	10.958	1016313	51.350
2	13.159	962875	48.650

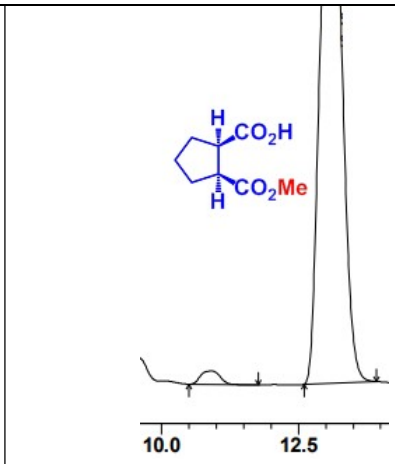

	Retention time	Area	Area %
1	10.917	52364	2.268
2	13.136	2256456	97.732

Fig. 19. HPLC chromatograms of racemic and (1*R*, 2*S*)-*cis*-2-Methoxycarbonyl-cyclopentane-1-carboxylic acid.

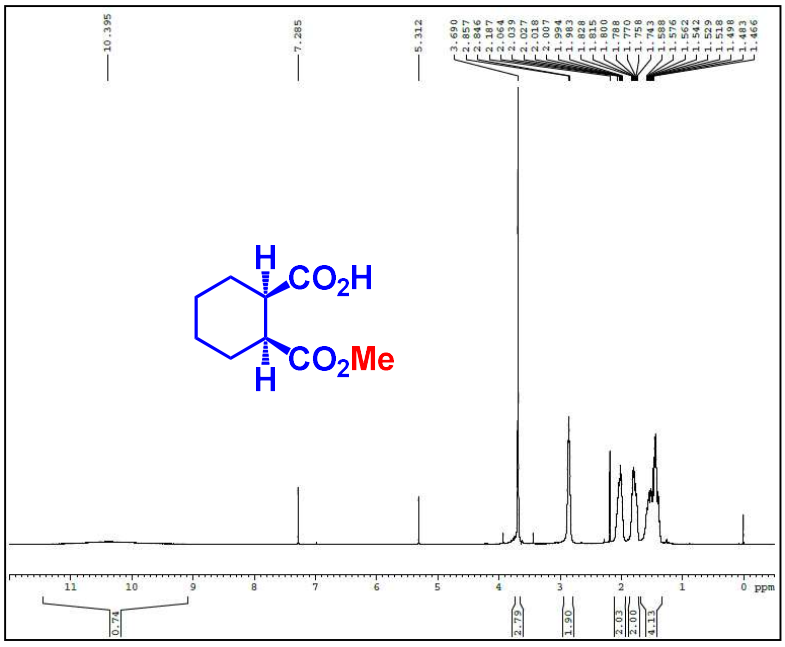

Fig. 20. ^{1}H NMR of (1R, 2S)-2-(methoxycarbonyl)-cyclohexane-1-carboxylic acid

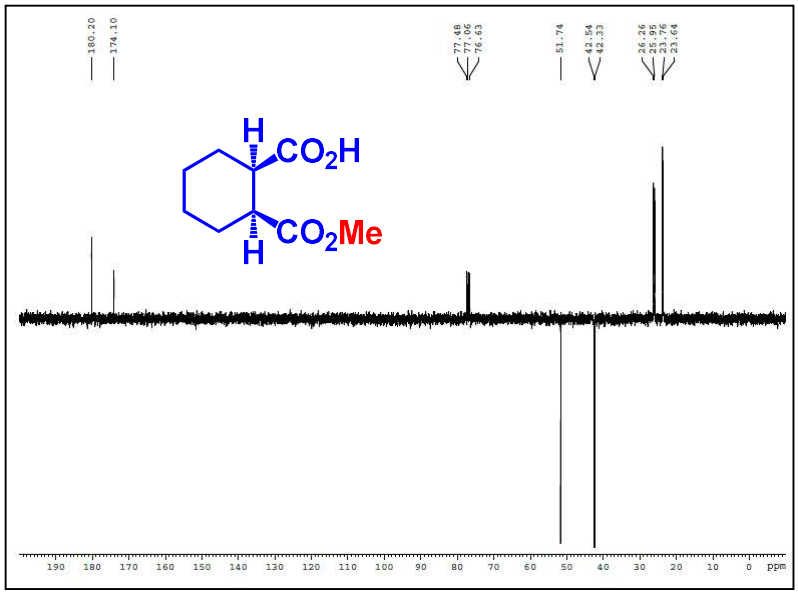

Fig. 21. ^{13}C NMR of (1R, 2S)-2-(methoxycarbonyl)-cyclohexane-1-carboxylic acid.

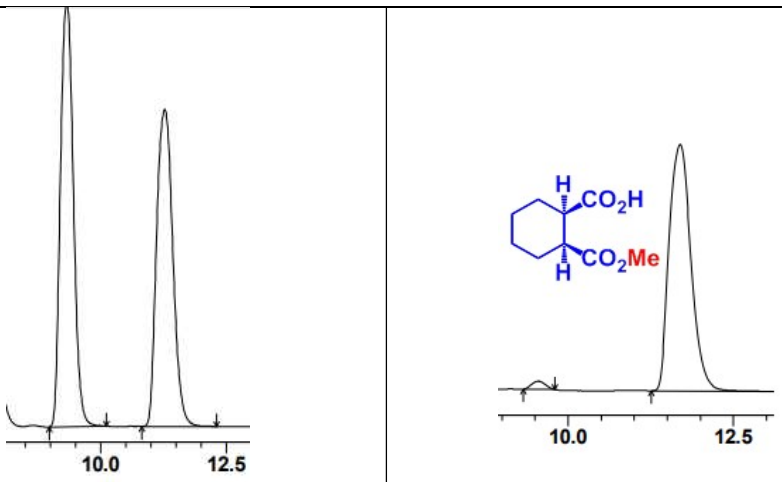

	Retention time	Area	Area %
1	9.326	995491	51.684
2	11.376	930633	48.316

	Retention time	Area	Area %
1	9.337	389282	3.112
2	11.382	12056858	96.385

Fig. 22. HPLC chromatograms of racemic and (1R, 2S)-2-(methoxycarbonyl)cyclohexane-1-carboxylic acid.

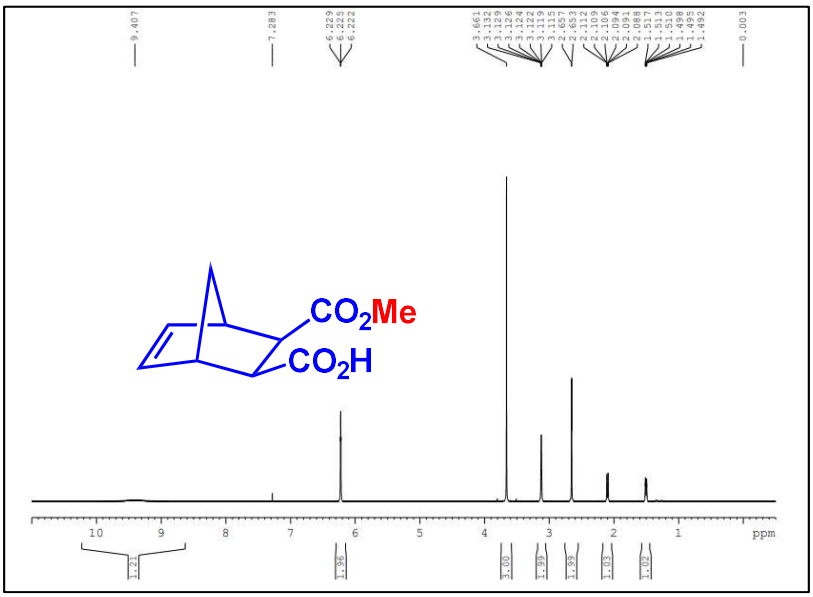

Fig. 23. ^{1}H NMR of (1R,2R,3S,4S)-3-(methoxycarbonyl)bicyclo[2.2.1]heptane-2-carboxylic acid

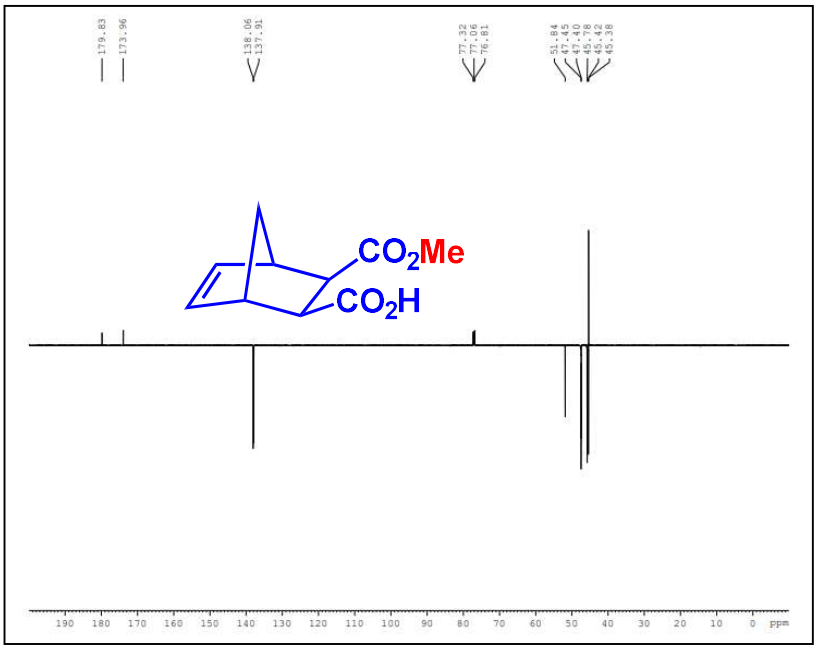

Fig. 24. ^{13}C NMR of (1R,2R,3S,4S)-3-(methoxycarbonyl)bicyclo[2.2.1]heptane-2-carboxylic acid

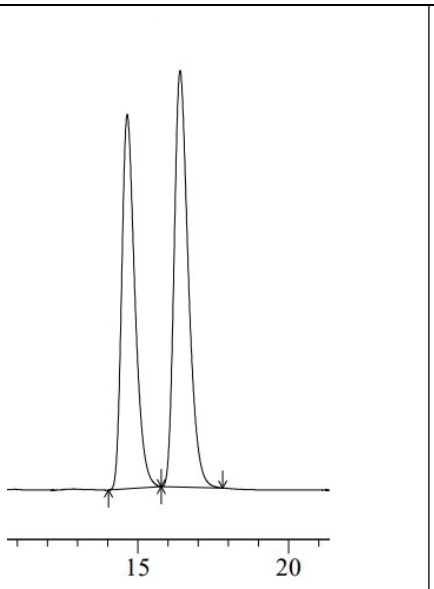

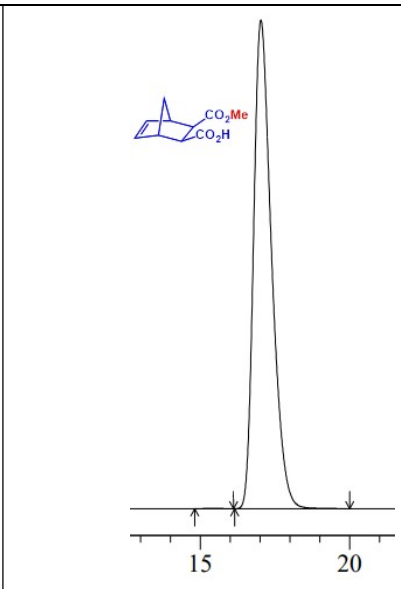

	Retention time	Area	Area %
1	14.656	285236	48.3
2	16.452	305315	51.7

	Retention time	Area	Area %
1	15.482	8250	0.9
2	17.063	908368	99.1

Fig. 25. HPLC chromatograms of racemic and (1R,2R,3S,4S)-3-(methoxycarbonyl) bicyclo-[2.2.1]heptane-2-carboxylic acid

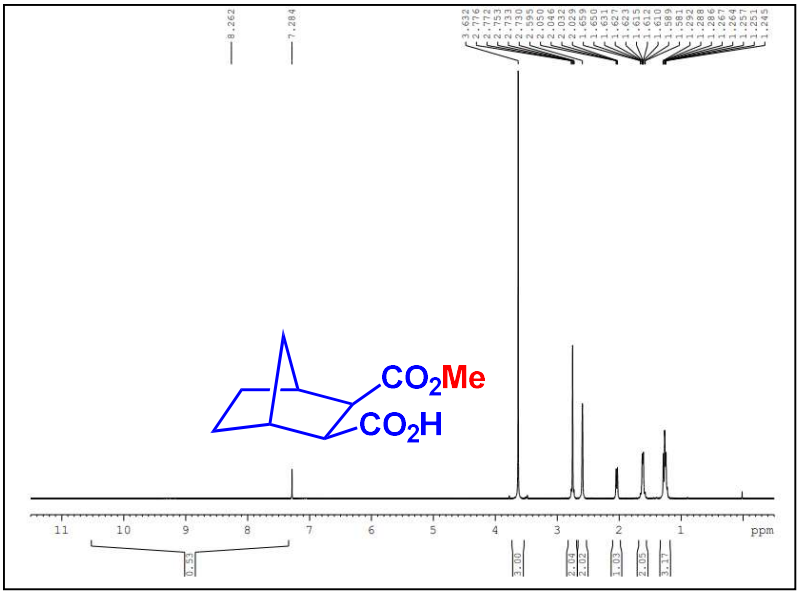

Fig. 26. ^{1}H NMR of (1R,2R,3S,4S)-3-(methoxycarbonyl)bicyclo[2.2.1]heptane-2-carboxylic acid

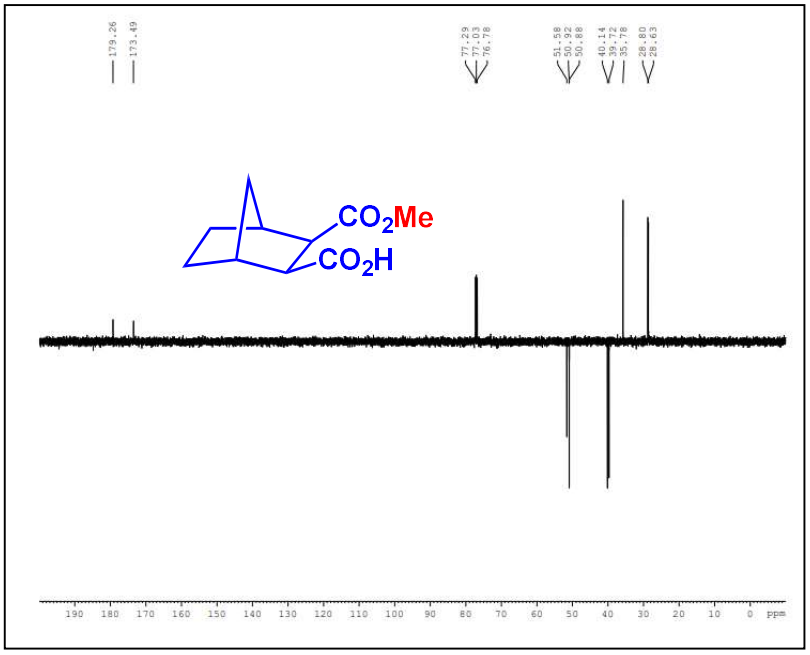

Fig. 27. ^{13}C NMR of (1R,2R,3S,4S)-3-(methoxycarbonyl)bicyclo[2.2.1]heptane-2-carboxylic acid

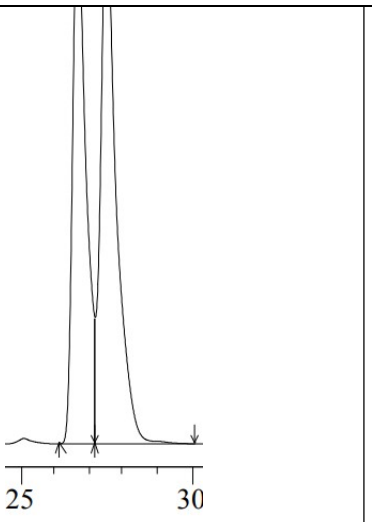

	Retention time	Area	Area %
1	26.768	663542	49.2
2	27.673	685121	50.8

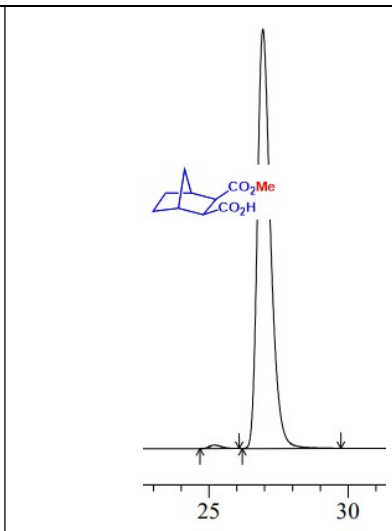

	Retention time	Area	Area %
1	25.264	7921	1.8
2	26.952	432156	98.2

Fig. 28. HPLC chromatograms of racemic and (1R,2R,3S,4S)-3-(methoxycarbonyl) bicyclo-[2.2.1]heptane-2-carboxylic acid

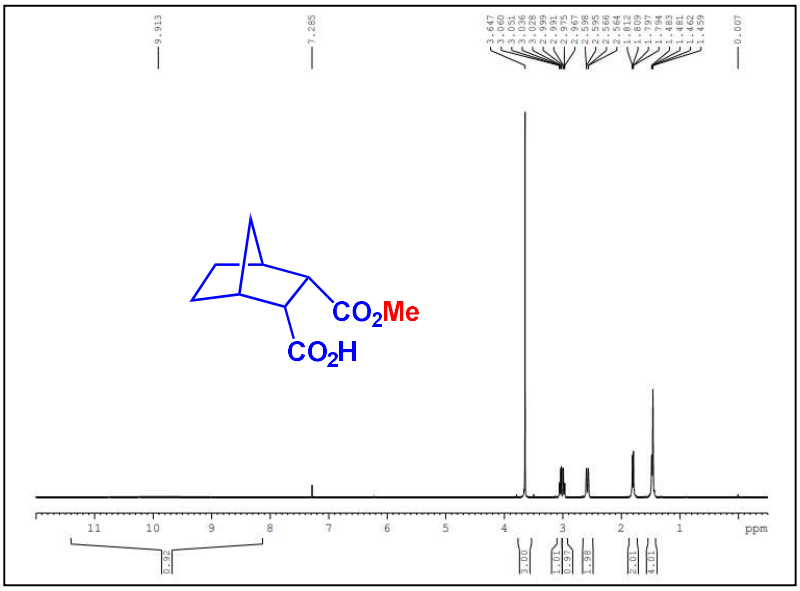

Fig. 29. ^{1}H NMR of (1R,2R,3S,4S)-3-(methoxycarbonyl)bicyclo[2.2.1]heptane-2-carboxylic acid

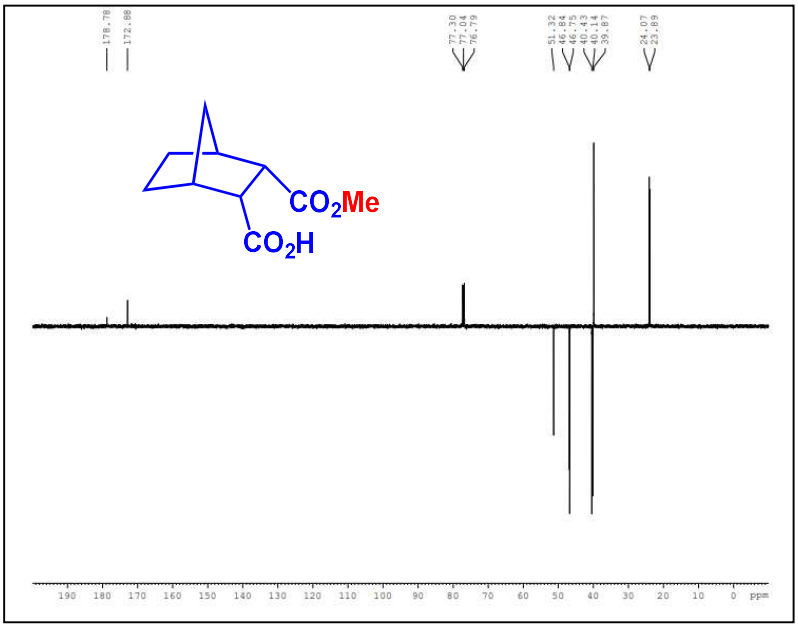

Fig. 30. ^{13}C NMR of (1R,2R,3S,4S)-3-(methoxycarbonyl)bicyclo[2.2.1]heptane-2-carboxylic acid

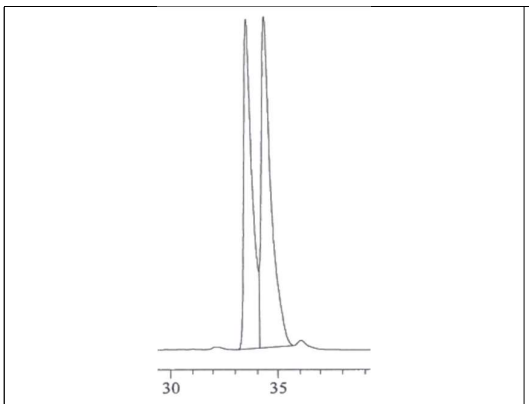

	Retention time	Area	Area %
1	33.365	570264	49.3
2	34.184	586458	50.7

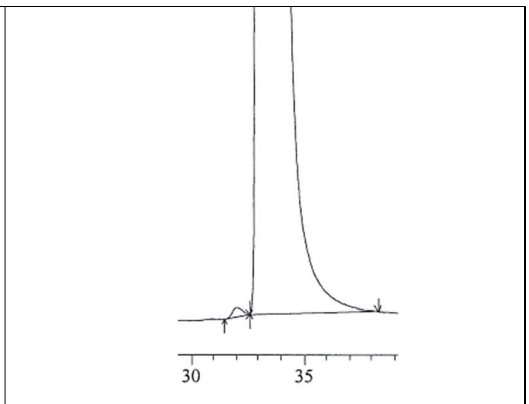

	Retention time	Area	Area %
1	32.016	13337	2.0
2	33.691	653523	98.0

Fig. 31. HPLC chromatograms of racemic and (1R,2R,3S,4S)-3-(methoxycarbonyl)bicyclo-[2.2.1]heptane-2-carboxylic acid

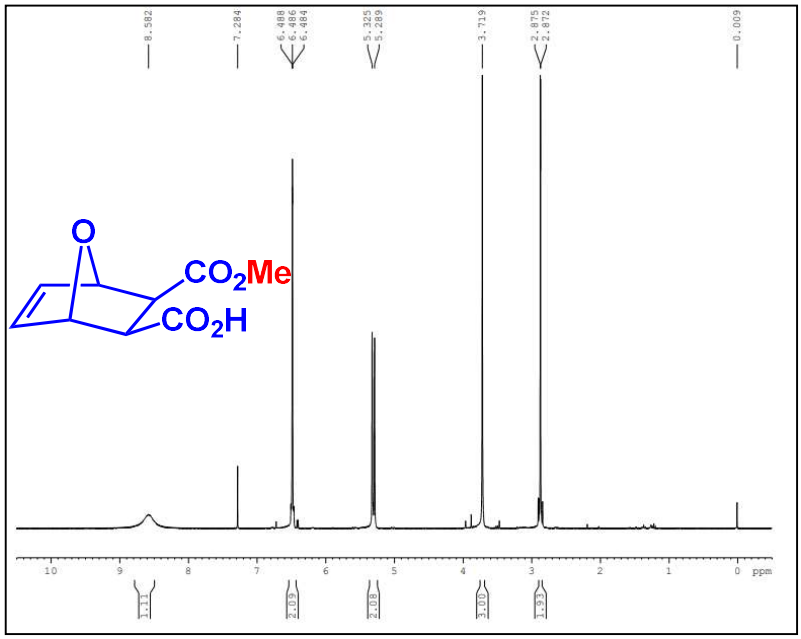

Fig. 32. 1H NMR of (1S,2R,4R)-3-(methoxycarbonyl)-7-oxabicyclo[2.2.1]hept-5-ene-2-carboxylic acid

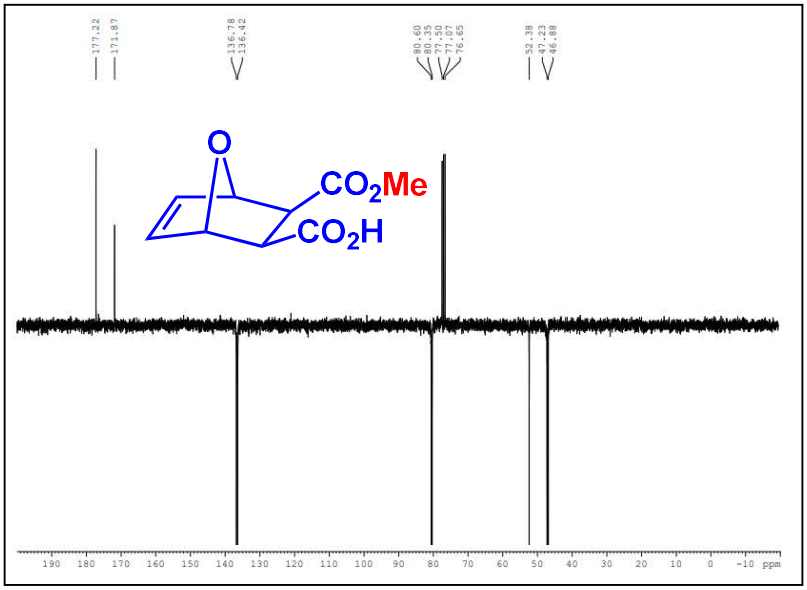

Fig. 33. ^{13}C NMR of (1S,2R,4R)-3-(methoxycarbonyl)-7-oxabicyclo[2.2.1]hept-5-ene-2-carboxylic acid

	Retention time	Area	Area %
1	27.36	817426	48.6
2	29.15	864521	51.4

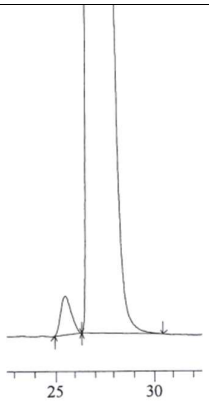

	Retention time	Area	Area %
1	25.52	9438	1.36
2	27.18	684561	98.64

Fig. 34. HPLC chromatograms of racemic and (1S,2R,4R)-3-(methoxycarbonyl)-7-oxabicyclo[2.2.1]hept-5-ene-2-carboxylic acid

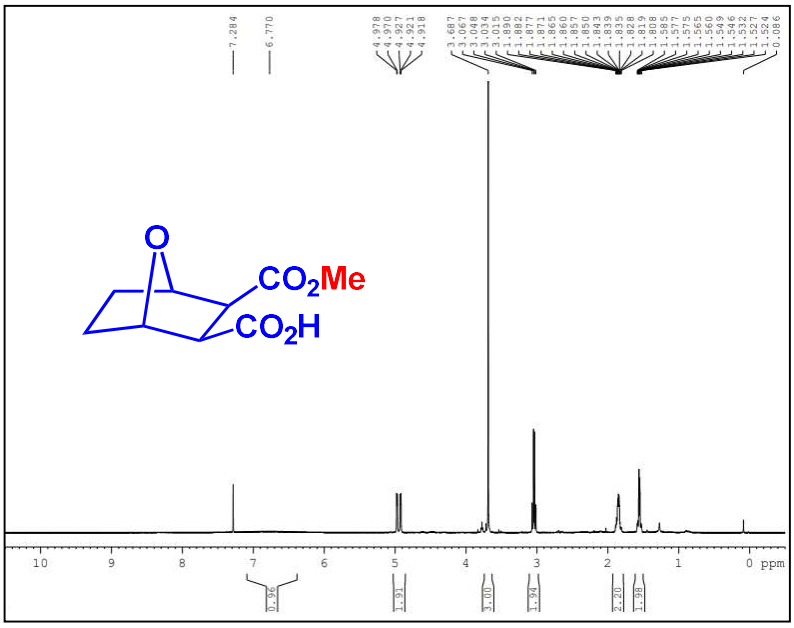

Fig. 35. 1H NMR of (1S,2R,4R)-3-(methoxycarbonyl)-7-oxabicyclo[2.2.1]heptane-2-carboxylic acid

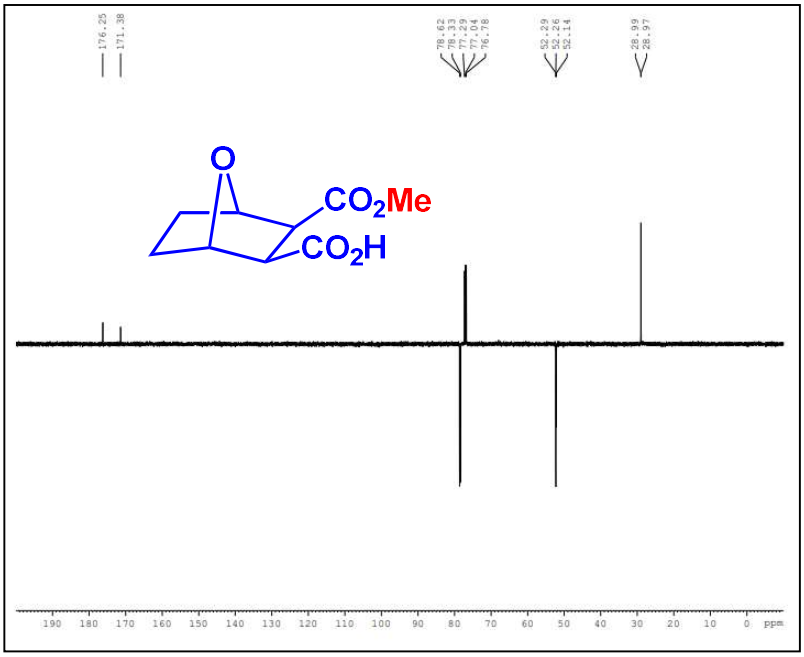

Fig. 36. ^{13}C NMR of (1S,2R,4R)-3-(methoxycarbonyl)-7-oxabicyclo[2.2.1]heptane-2-carboxylic acid

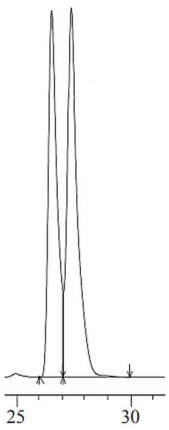

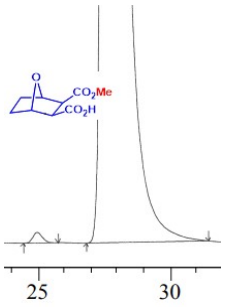

	Retention time	Area	Area %
1	26.630	458643	49.8
2	27.482	462327	50.2

	Retention time	Area	Area %
1	26.002	5343	1.48
2	26.835	355654	98.52

Fig. 37. HPLC chromatograms of racemic and (1S,2R,4R)-3-(methoxycarbonyl)-7-oxabicyclo[2.2.1]heptane-2-carboxylic acid

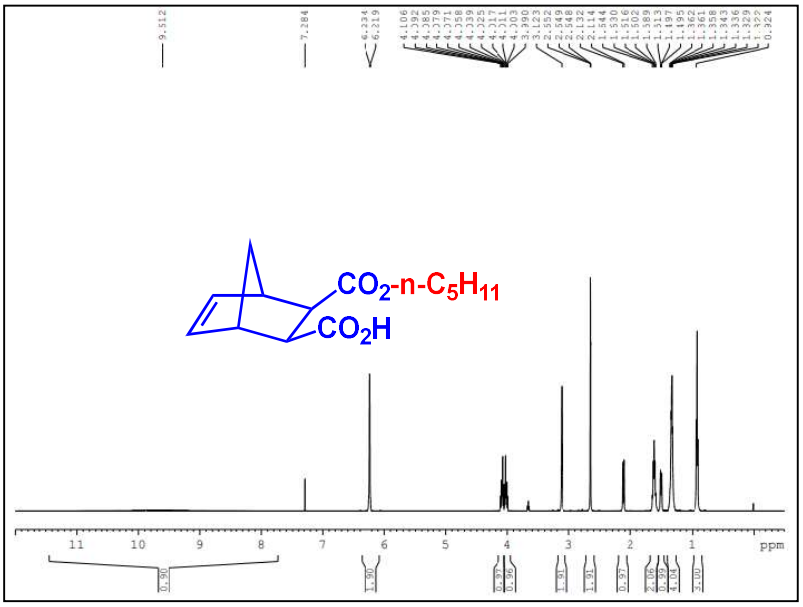

Fig. 38. 1H NMR of (1S, 2S, 4R)-3-((pentyloxy)carbonyl)bicyclo[2.2.1]hept-5-ene-2-carboxylic acid

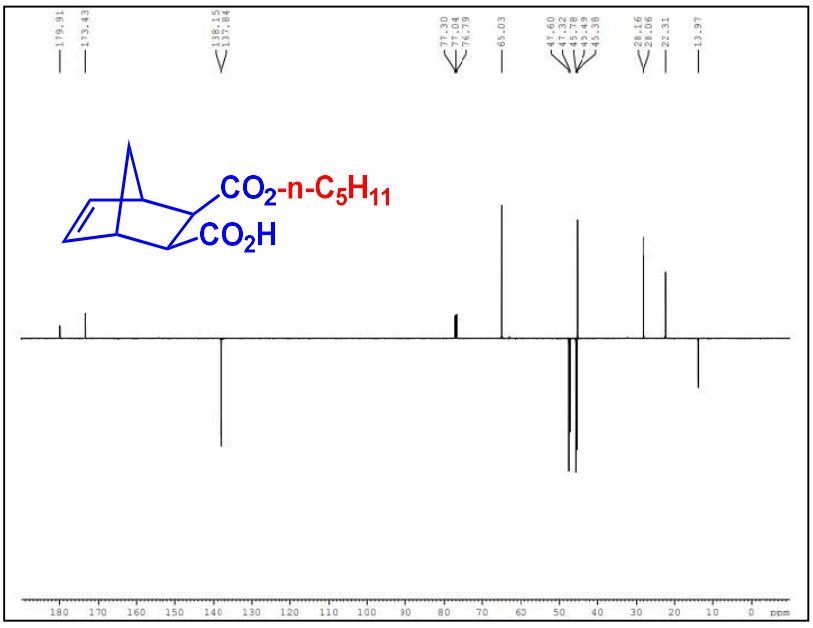

Fig. 39. 13C NMR of (1S, 2S, 4R)-3-((pentyloxy)carbonyl)bicyclo[2.2.1]hept-5-ene-2-carboxylic acid

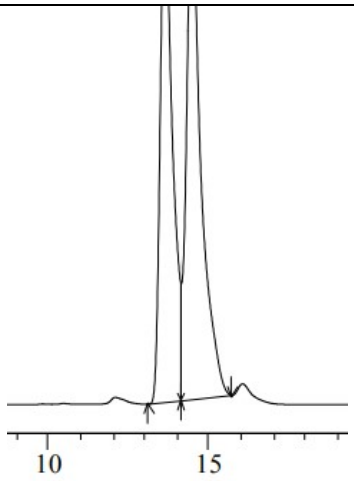

	Retention time	Area	Area %
1	13.62	4421002	45.94
2	14.46	5201169	54.05

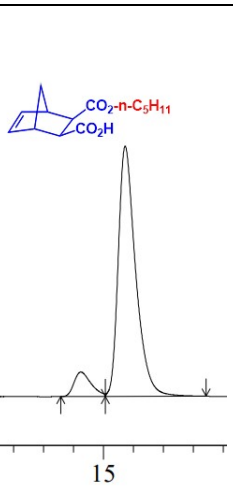

	Retention time	Area	Area %
1	14.24	197928	8.75
2	15.72	2062250	91.24

Fig. 40. HPLC chromatographs of racemic and (1S, 2S, 4R)-3-((pentyloxy) carbonyl)bicyclo [2.2.1]hept-5-ene-2-carboxylic acid.

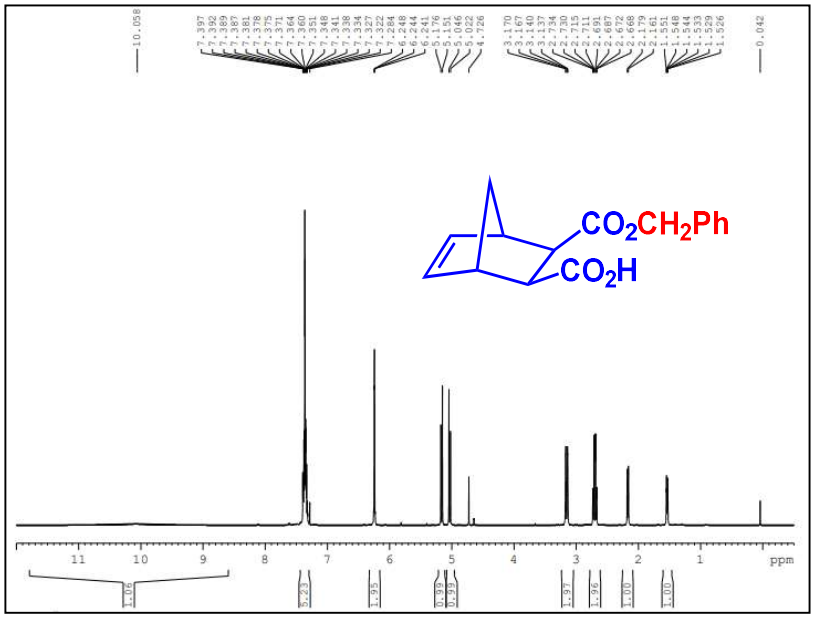

Fig. 41. 1H NMR of (1S, 2S, 4R)-3-((benzyloxy)carbonyl)bicyclo[2.2.1]hept-5-ene-2-carboxylic acid.

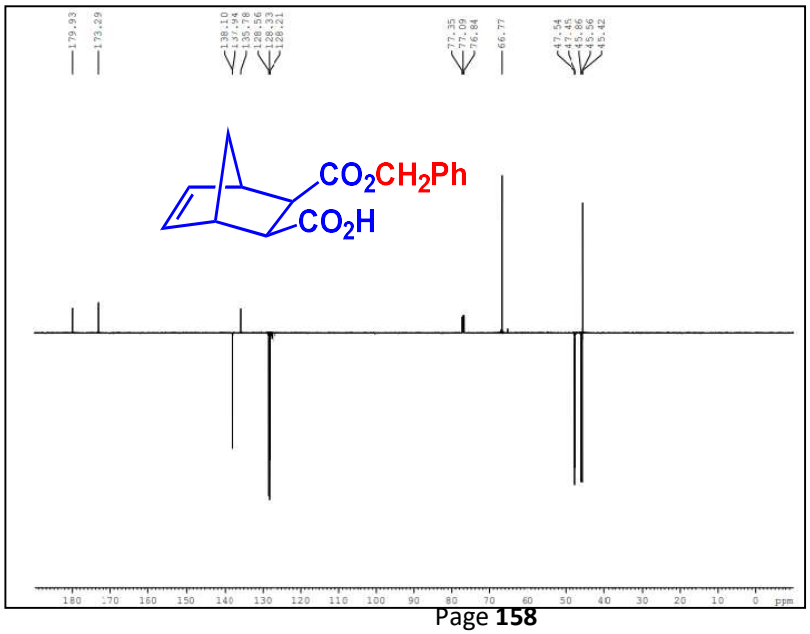

Fig. 42. 13C NMR of (1S, 2S, 4R)-3-((benzyloxy)carbonyl)bicyclo[2.2.1]hept-5-ene-2-carboxylic acid.

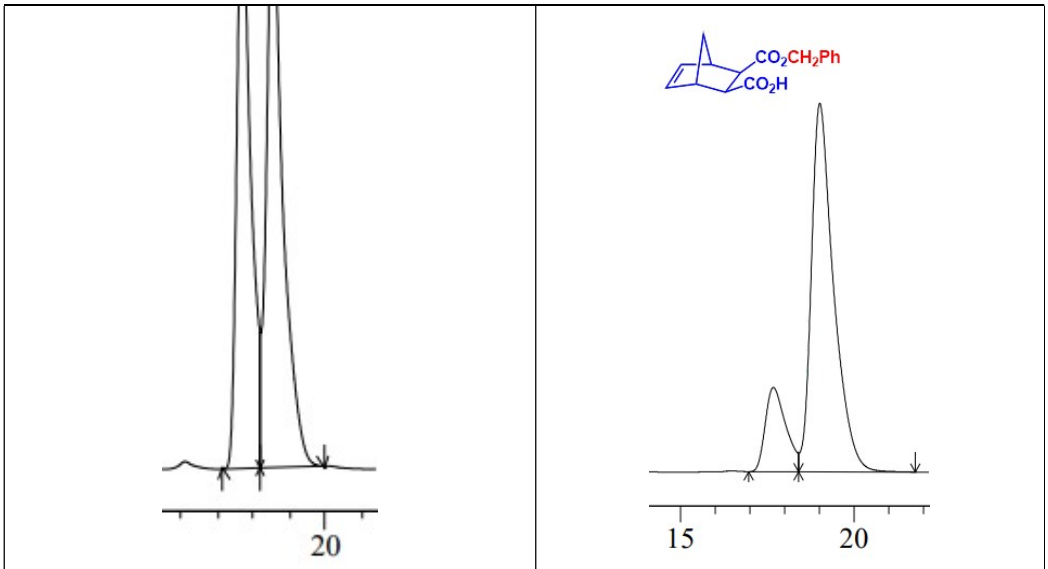

	Retention time	Area	Area %
1	17.6	4338839	48.3
2	18.8	4644265	51.7

	Retention time	Area	Area %
1	17.8	618394	17.44
2	19.0	2926603	82.55

Fig. 43. HPLC chromatographs of racemic and (1S, 2S, 4R)-3 ((benzyloxy)carbonyl)bicyclo [2.2.1]hept-5-ene-2-carboxylic acid.

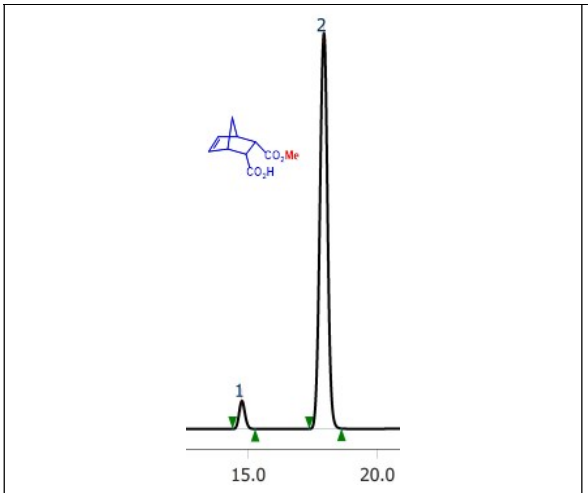

	Retention time	Area	Area %
1	14.843	1346183	3.244
2	18.113	40148959	96.756

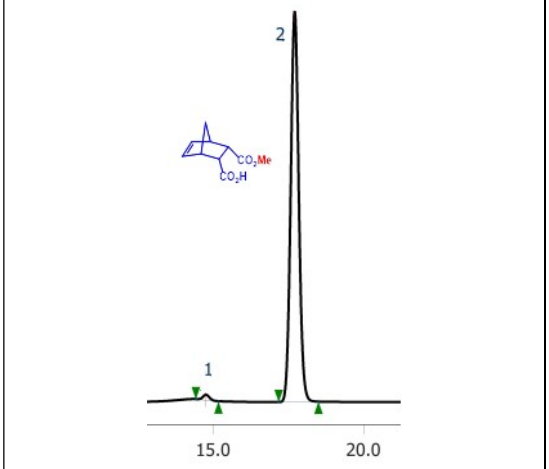

	Retention time	Area	Area %
1	14.883	271208	2.125
2	18.133	12491520	97.875

Fig. 44. HPLC chromatograms of racemic and (2*R*, 3*S*)-3-*endo*-Methoxycarbonyl-bicyclo[2.2.1]hept-5-ene-2-*endo*-carboxylic acid synthesized at 25 and 0°C.

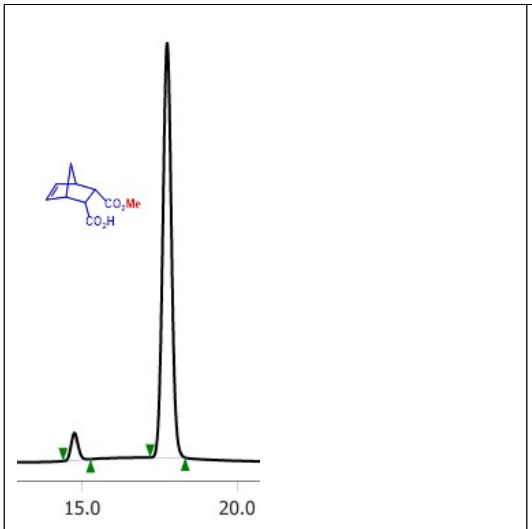

	Retention time	Area	Area %
1	14.887	855445	3.157
2	18.173	26241343	96.843

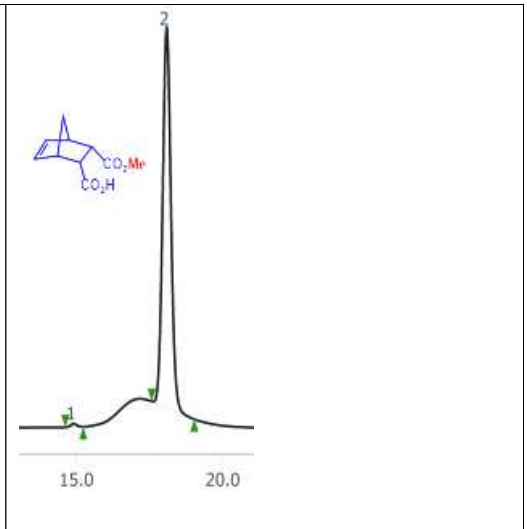

	Retention time	Area	Area %
1	14.850	292011	1.28
2	18.168	22521377	98.72

Fig. 45. HPLC chromatograms of racemic and (2*R*, 3*S*)-3-*endo*-Methoxycarbonyl-bicyclo[2.2.1]hept-5-ene-2-*endo*-carboxylic acid synthesized after using the catalyst 10 and 5 cycles.

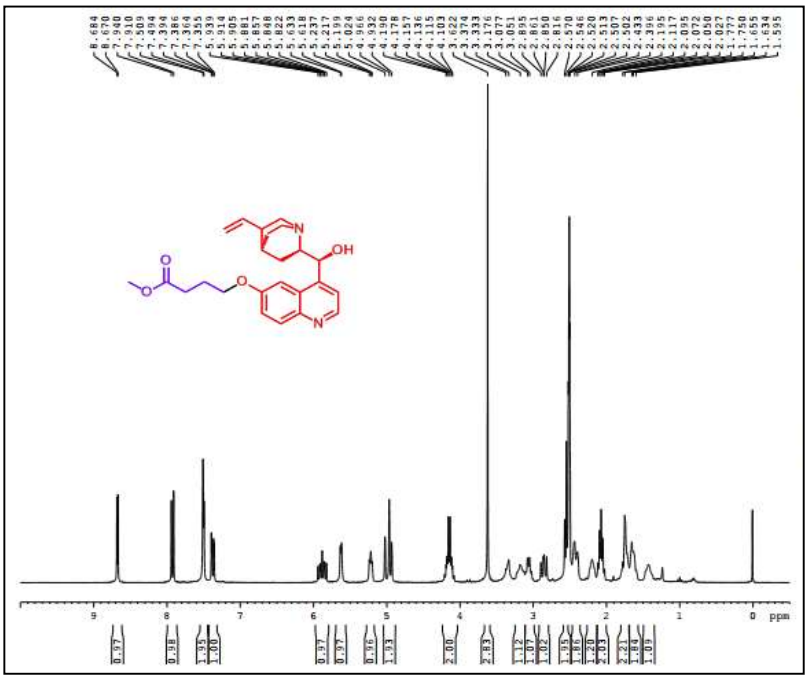

Fig. 46. ^{1}H NMR of 4-((4-((1S)-hydroxy((2R,4S,5R)-5-vinylquinuclidin-2-yl)methyl) quinolin-6-yl)oxy)butanoic acid methyl ester.

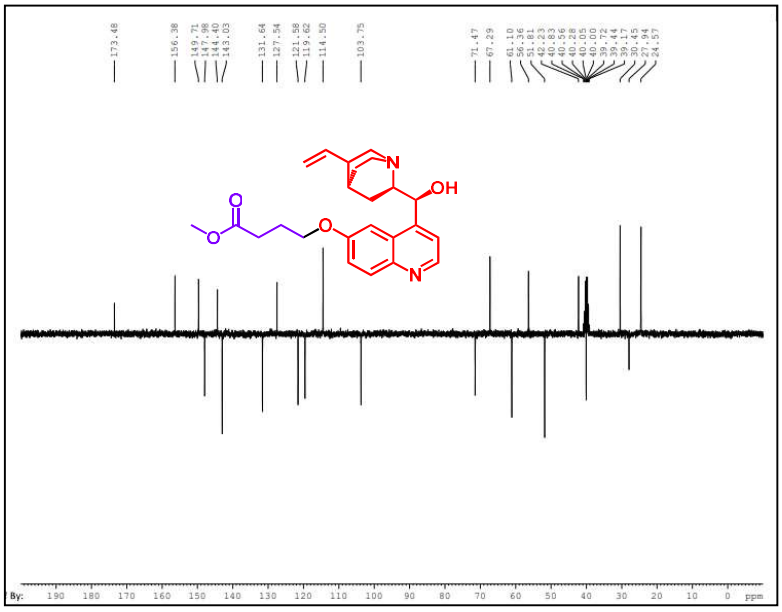

Fig. 47. ^{13}C NMR of 4-((4-((1S)-hydroxy((2R,4S,5R)-5-vinylquinuclidin-2-yl)methyl) quinolin-6-yl)oxy)butanoic acid methyl ester.

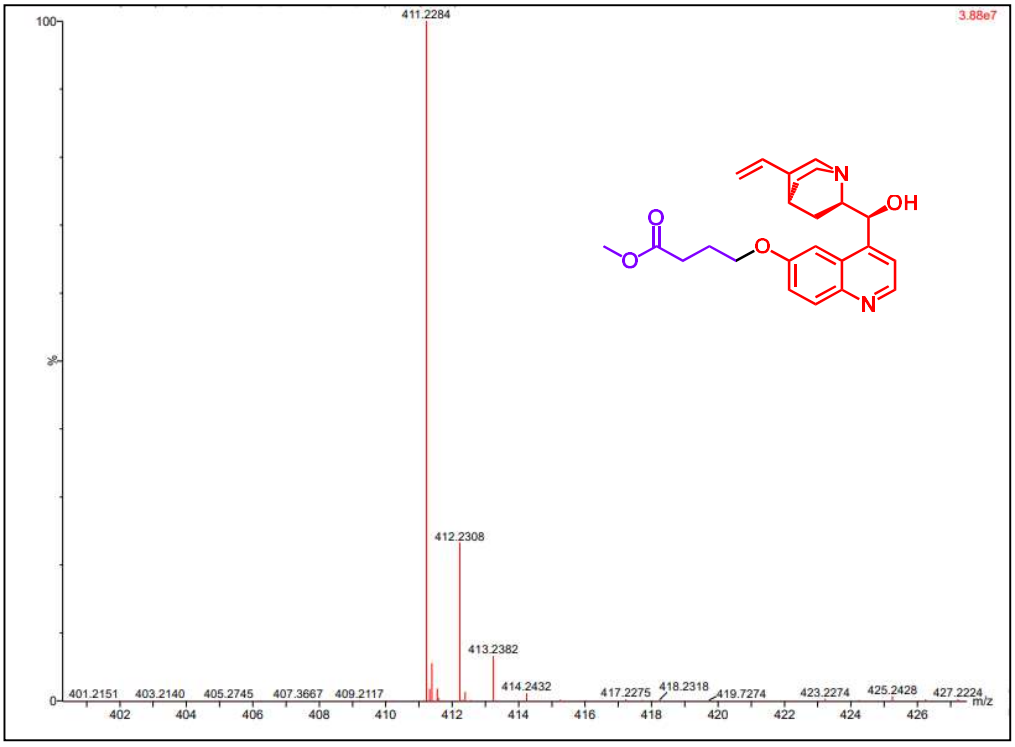

Fig. 48. HRMS of 4-((4-((1S)-hydroxy((2R,4S,5R)-5-vinylquinuclidin-2-yl)methyl) quinolin-6-yl)oxy)butanoic acid methyl ester.

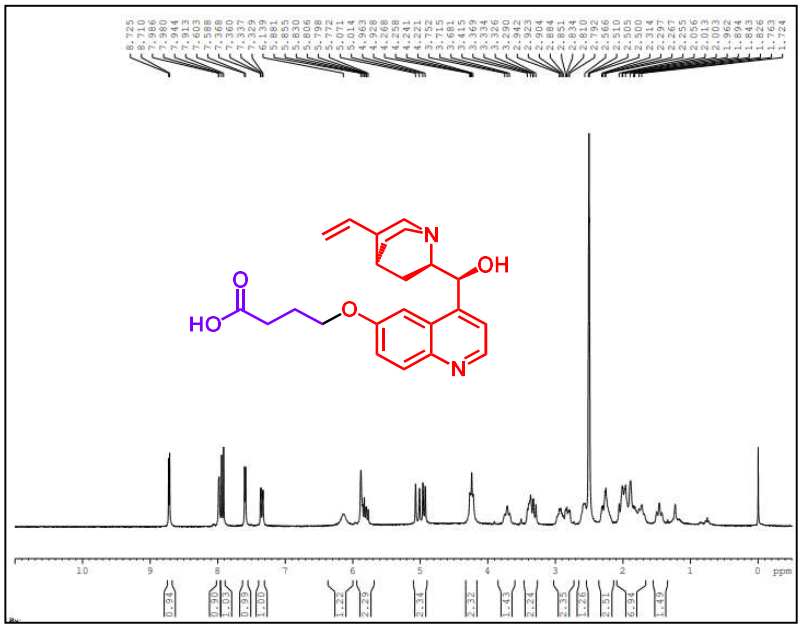

Fig. 49. ^{1}H NMR of 4-((4-((1S)-hydroxy((2R,4S,5R)-5-vinylquinuclidin-2-yl)methyl) quinolin-6-yl)oxy)butanoic acid.

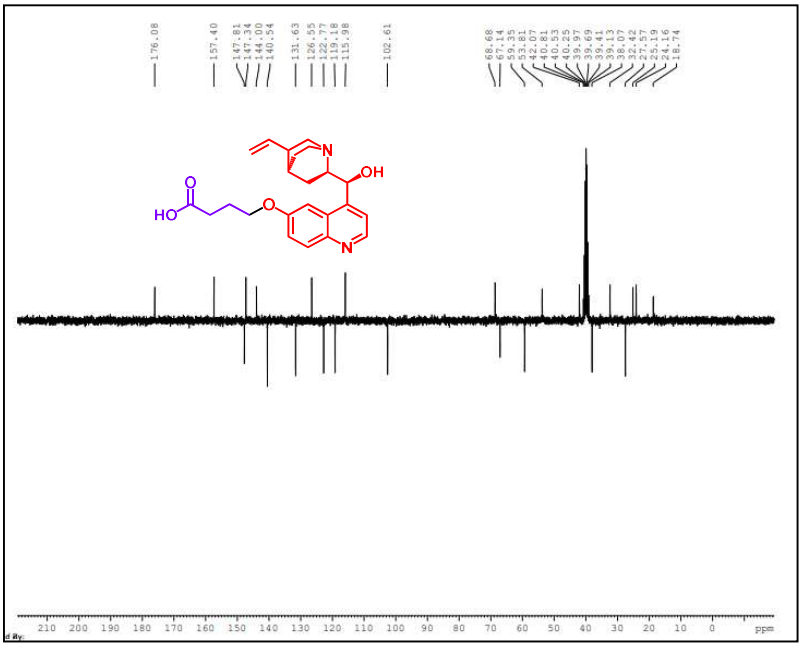

Fig. 50. ^{13}C NMR of 4-((4-((1S)-hydroxy((2R,4S,5R)-5-vinylquinuclidin-2-yl)methyl) quinolin-6-yl)oxy)butanoic acid.

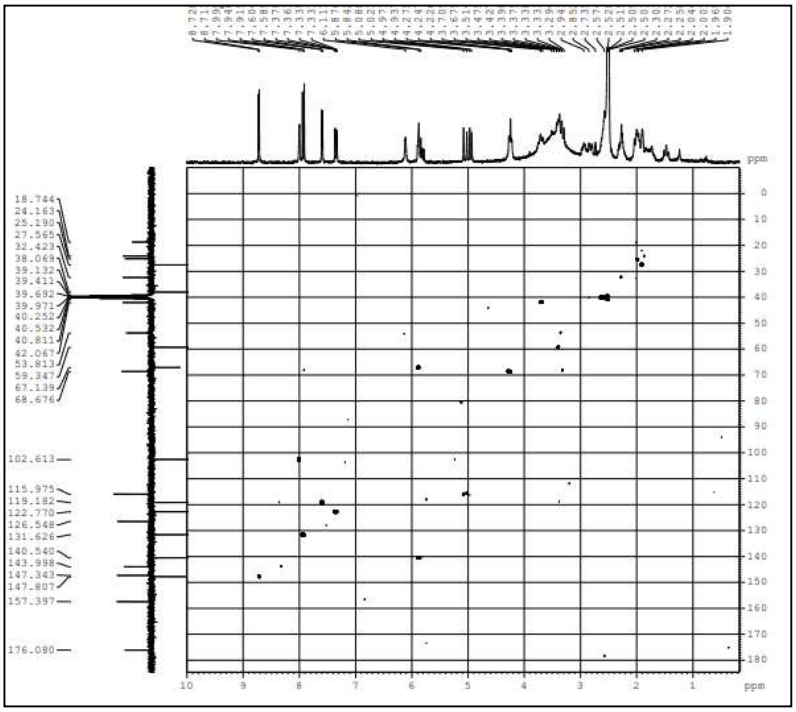

Fig. 51. HSQC of 4-((4-((1S)-hydroxy((2R,4S,5R)-5-vinylquinuclidin-2-yl)methyl)quinolin-6-yl)oxy)butanoic acid.

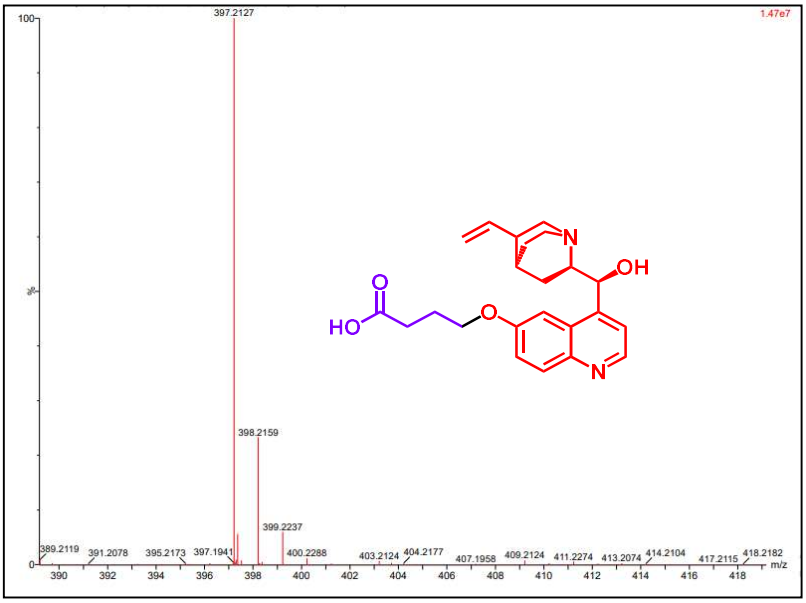

Fig. 52. HRMS of 4-((4-((1S)-hydroxy((2R,4S,5R)-5-vinylquinuclidin-2-l)methyl)quinolin-6-yl) oxy)butanoic acid.

4.4. Conclusion

We have demonstrated that the enantioselective *meso*-cyclic anhydride ring opening by alcoholysis can be carried out in a highly efficient and selective way by systematic modification in the cinchona alkaloid's molecular framework and by adsorbing the same on the surface of magnetic Fe_3O_4 NPs to ease the recovery and recycling of the catalyst. The optimization of reaction parameters of model ERO by alcoholysis establishes that the developed protocol results up to 97% yield with 98% ee of chiral hemiester when the reaction is carried out at -45 ^oC in diethyl ether as a solvent for 60 h in the presence of a catalytic amount of Fe_3O_4@mQD NPs. By implementing all the optimized process parameters for pilot-scale production of chiral hemiester, it can be concluded that (i) the developed process becomes cost-effective compared to other processes due to the requirement of less amount of catalyst (ii) catalyst recovery becomes easy by applying a simple bar magnet (iii) the problem of protonation of catalytic quinidine nitrogen by the product hemiester gets nullified due to proper molecular orientation of QD on adsorption keeping the distance between catalytic site, substrate and the product formed (iv) the as-synthesized catalyst NPs maintained their efficiency for five cycles without significant loss in % yield and selectivity. Absorption and emission spectroscopies, chiroptical study, and surface probe microscopy revealed that spatial molecular orientation of the chiral molecule on adsorption could induce a proper molecular orientation by intermolecular hydrogen bonding, in turn, making the achiral magnetic surface chiral. These chirality-induced magnetic surfaces can be exploited for enantioselective organic transformations. This study opens new avenues for the development of chiral magnetic surfaces that can be used for efficient stereoselective heterogeneous catalysis.

4.5. References

1. I. Atodiresei, I. Schiffers and C. Bolm, *Chem. Rev.,* 2007, **107**, 5683-5712.

2. Y. G. Chen, P. McDaid ans L. Deng, *Chem. Rev.*, 2003, **103**, 2965-298.

3. R. Borrmann, V. Palchyk, A. Pich and M. Rueping, *ACS Catal.*, 2018, **8**, 7991−7996.

4. T. Ivšić, I. Dokli, A. Rimac and Z. Hameršak, Eur. J. Org. Chem., 2014, 631-638.

5. X. Huang, S. Broadbent, C. Dvorak and S. Zhao, *Org. Process Res. Dev.*, 2010, **14**, 612- 616.

6. M. C. Willis, *J. Chem. Soc., Perkin Trans.*, 1999, **1**, 1765-1784.

7. M. W. Goldberg and L. H. Sternbach, U.S. Patent 2,489,232, 1949; Chem. Abstr. 1951, 45, 184.

8. C. Choi, S. -K. Tian and L. Deng, Synthesis, 2001, 1737-1741.

9. D. Raederstorff, A. Y. L. Shu, J. E. Thompson and C. Djerassi, *J. Org. Chem.*, 1987, **,** 2337-2346.

10. B. A. Kulkarni, S. Chattopadhyay, A. Chattopadhyay and V. R. Mamdapur, *J. Org. Chem.*, 1993, **58**, 5964-5966.

11. H. Ogawa, T. Chihara and K. Taya, *J. Am. Chem. Soc.*, 1985, **107**, 1365-1369.

12. S. O. Tomer and H. P. Soni, *Org. Biomol. Chem.*, 2017, **15**, 8990-8997.

13. U. T. Bornscheuer and R. J. Kazlauskas, *Hydrolases in Organic Synthesis: Regio and Stereoselective Biotransformations.* Wiley-VCH: Weinheim. 1999.

14. M. Hazama, T. Aratani, G. Suzukamo and T. Takahashi, Eur. Pat., EP 0 044 158 A1, 1982.

15. J. Hiratake, M. Inagaki, Y. Yamamoto and J. Oda, *Chem. Soc. Perkin Trans.*, 1987, **1**, 1053-1058.

16. D. Seebach, G. Jaeschke and Y. M. Wang, *Angew. Chem. Int. Ed. Engl.,* 1995, **34**, 2395 - 2396.

17. G. Jaeschke and D. Seebach, *J. Org. Chem.*, 1998, **63**, 1190-1197.

18. P. Gopinath, T. Watanabe and M. Shibasaki, *Org. Lett.*, 2012, **14**, 1358-1361.

19. H. Imado, T. Ishizuka and T. Kunieda, Tetrahedron Lett., 1995, **36**, 931-934.

20. N. Hashimoto, S. Kawamura, T. Ishizuka and T. Kunieda, Tetrahedron Lett., 1996, **37**, 9237-9240.

21. C. Bolm, C. L. Dinter, A. Seger, H. Hoecker and J. Brozio, *J. Org. Chem.*, 1999, **64**, 5730-5731.

22. B. Rodriguez, T. Rantanen and C. Bolm, *Angew. Chem.*, 2006, **118**, 7078-7080.

23. Y. Chen, S. -K. Tian and L. Deng, *J. Am. Chem. Soc.*, 2000, **122**, 9542-9543.

24. T. P. Yoon and E. N. Jacobsen, *Science*, 2003, **299**, 1691-1693.

25. M. Tommaso, *WIREs Comput. Mol. Sci., 2011,* **1**, 142-152.

26. J. Duan and P. Li, *Catal. Sci. Technol.*, 2014, **4**, 311-320.

27. J. Hiratake, Y. Yamamoto and J. Oda, *Chem. Soc. Chem. Commun.*, 1985, 1717-1719.

28. R. A. Aitken, J. Gopal and J. A. Hirst, *J. Chem. Soc., Chem. Commun.*, 1988, 632 -634.

29. R. A. Aitken and J. Gopal, *Tetrahedron: Asymmetry*, 1990, **1**, 517-520.

30. C. Bolm, A. Gerlach and C. L. Dinter, Synlett, 1999, **2**, 195-196.

31. C. Bolm, C. L. Dinter, A. Seger, H. Höecker and J. Brozio, *J. Org. Chem.*, 1999, **64**, 5730-5731.

32. R. Jenkins and R. L. Snyder, *Introduction to X-ray PowderDiffractometry.* John Wiley & Sons, NewYork. 1996.

33. K. S. W. Sing, D. H. Everett, R. A. W. Haul, L. Moscou, R. A. Pierotti, J. Rouquerol and T. Siemieniewska, *Pure Appl. Chem.*, 1985, **57**, 603-619.

34. J. Yu, L. Zhang, B. Cheng and Y. Su, *J. Phys. Chem. C*, 2007, **111**, 10582-10589.

35. E. Shah and H. P. Soni, *RSC Adv.*, 2013, **3**, 17453-17461.

36. E. Shah, P. Upadhyay, M. Singh, M. S. Mansuri, R. Begum, N. Sheth and H. P. Soni, *New J. Chem.*, 2016, **40**, 9507-9519.

37. M. Kakihana, T. Nagumo, O. Makoto and H. Kakihana, *J. Phys. Chem.*, 1987, **91**, 6128-6136.

38. C. Bolm, I. Schiffers, C. L. Dinter and A. Gerlach, *J. Org. Chem.*, 2000, **65**, 6984 -6991.

39. H. Li, X. Liu, F. Wu, L. Tang and L. Deng, PNAS, 2010, **107**, 20625-20629.

40. R. P. Jumde, A. D. Pietro, A. Manariti and A. Mandoli, *Chem. Asian J.*, 2015, **10**, 397-404.

41. F. Bigi, S. Carloni, R. Maggi, A. Mazzacani, G. Sartori and G. Tanzi, *J. Mol. Catal. A: Chemical,* 2002, **182-183**, 533-539.

42. L. Sarda and P. Desnuelle, *Biochim Biophys Acta.*, 1958, **30**, 513-521.

43. D. Blow, *Nature*, 1990, **343**, 694-695.

44. E. Shah, P. Mahapatra, A. V. Bedekar and H. P. Soni, *RSC Adv.*, 2015, **5**, 26291-26300.

45. H. Yang, and M. W. Wong, *J. Am. Chem. Soc.*, 2013, **135**, 5808-5818.

46. B. Mitschke, M. Turberg and B. List, *Chem,* 2020, **6**, 2515-2532.

47. B. Dedeoglu, S. Catak, A. Yildirim, C. Bolm and V. Aviyente, *ChemCatChem*, 2015, **7**, 4173 – 4179.

48. J. Gawronski, M. Brzostowska and J. Koput, *Croat. Chem. Acta*, 1989, **62**, 97-107.

49. A. Loudet and K. Burgess, *Chem. Rev.*, 2007, **107**, 4891–4932.

50. J. Mei, Y. Hong, J. W. Y. Lam, A. Qin, Y. Tang and B. Z. Tang, *Adv. Mater.*, 2014, **26**, 5429-5479.